ARTICLE

https://doi.org/10.1590/2317-4889202120200051

BJGEO Brazilian Journal of Geology

Magnetic and radiometric signatures of alkaline rocks and gabbros from the Ponta Grossa Arch, southeastern Paraná Basin, Brazil

Vinicius Antunes Ferreira da Silva[1]*, Francisco José Fonseca Ferreira[1]

Abstract

We present airborne magnetic and radiometric characteristics of some igneous suites from the Ponta Grossa Arch Alkaline Province (southern Brazil), namely the Bairro da Cruz, Banhadão, Barra do Itapirapuã, Mato Preto and Tunas complexes, Barra do Teixeira Phonolite, Itapirapuã Nepheline syenite, and José Fernandes Gabbro. We applied magnetic susceptibility 3D inversions using the total magnetic anomaly data together with its analytic signal of the vertical integral and the vertical integral of the analytic signal for the Bairro da Cruz, José Fernandes, and Tunas intrusions. Gamma-ray spectrometric methods involved analyses of basic, ternary, and ratio maps, thorium-normalized parameters, and radioelement concentrations at sampled data points. Stacked profiles from geophysical data were generated for each rock. The Bairro da Cruz, José Fernandes, and Tunas intrusions are associated with dipolar anomalies with normal polarity whereas their inversions show low magnetic susceptibility values. Gamma-ray spectrometric results allowed us to verify that all complexes are enriched mainly in eTh. Carbonatite bodies showed the highest contents of eTh and eU. Our findings are consistent with geophysical responses of alkaline bodies and impact the understanding of geophysical signatures, especially radiometric ones, of alkaline provinces in Brazil.

KEYWORDS: airborne gamma-ray spectrometry; aeromagnetics; Ponta Grossa Arch Alkaline Province; alkaline rocks; carbonatites.

INTRODUCTION

The Ponta Grossa Arch (PGA) is an uplifted domain located in the southeastern Paraná Basin and its Precambrian basement (Fig. 1). This arch hosts both alkaline and carbonatitic-alkalic intrusions. These complexes were studied by Almeida (1983), who labeled them as the Ponta Grossa Arch Alkaline Province (PGAAP). Most of this province is situated between the southern parts of the Guapiara (Ferreira *et al.* 1981) and São Jerônimo-Curiúva (Vieira 1973, Ferreira 1982) magnetic lineaments.

Alkaline intrusions have been recognized and detailed in different scales by airborne magnetic and gamma-ray spectrometric surveys. These surveys contribute to a variety of geological and geophysical interpretations and modeling applications, such as mapping of bedrocks and mineral exploration (Airo *et al.* 2014), as well as the discovery of uranium deposits in alkaline igneous complexes (*e.g.* Cercado Mine in Poços de Caldas, Forman and Angeiras 1981). For example, aeromagnetic maps aid the interpreter in verifying anomalies that coincide with outcropping alkaline intrusions, or even those with no surface expression, as well as to verify possible structural control on such intrusions (Marangoni and Mantovani 2013, Louro *et al.* 2019). As for radiometrics, alkaline rocks tend to enrich in equivalent thorium (eTh), which forms complex ions with sulfides, carbonates, and phosphates (Airo 2015). Furthermore, carbonatitic-alkalic complexes may show potential for rare earth elements (REE), niobium, and vermiculite mineralizations which are resources with economic importance for Brazil (Gomes and Comin-Chiaramonti 2005).

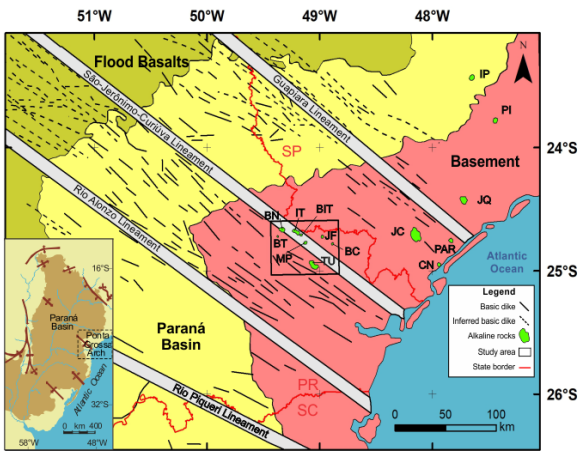

Source: modified from Ruberti *et al.* (2005) and Gomes *et al.* (2018).

Figure 1. Sketch map of the Ponta Grossa Arch Alkaline Province. Alkaline complexes: Bairro da Cruz (BC), Barra do Itapirapuã (BIT), Banhadão (BN), Barra do Teixeira (BT), Cananéia (CN), Ipanema (IP), Itapirapuã (IT), Jacupiranga (JC), José Fernandes (JF), Juquiá (JQ), Mato Preto (MP), Pariquera-Açu (PAR), Piedade (PI), and Tunas (TU). States: São Paulo (SP), Paraná (PR), and Santa Catarina (SC).

[1]Laboratory for Research in Applied Geophysics, Department of Geology, Universidade Federal do Paraná – Curitiba (PR), Brazil. E-mails: vinicius.anp@gmail.com, francisco.ferreira@ufpr.br

*Corresponding author.

Supplementary data

Supplementary data associated with this article can be found in the online version: Supplementary Material A, Supplementary Material B and Supplementary Material C.

The PGAAP was studied by Ulbrich and Gomes (1981), Almeida (1983) and several authors, including Comin-Chiaramonti and Gomes (2005), Gomes *et al.* (2011), and Gomes and Comin-Chiaramonti (2017), who did an extensive review about the Mesozoic-Cenozoic alkaline magmatism in the Brazilian platform. The area has also been studied by Marangoni and Mantovani (2013), who characterized state-of-the-art magnetic and gravity signatures in the PGAAP and other alkaline provinces in Brazil. However, these authors have not reported geophysical signatures of all the bodies from the PGAAP, describing only Ipanema, Jacupiranga, Juquiá, Pariquera-Açu, and Tunas. All the works compiled by these authors used previous and lower-resolution aerogeophysical data (*i.e.* flight lines spaced with 1 km or more) than the one used in this work.

Although a variety of geophysical studies were applied in Brazilian alkaline rocks, not all the provinces have been studied in detail by different geophysical methods. Little attention has been paid to the use of gamma-ray spectrometric data alongside the magnetic. Therefore, this study aimed to define what are the airborne magnetic and radiometric signatures of eight bodies in the PGAAP, namely: Bairro da Cruz (BC), Banhadão (BN), Itapirapuã (IT), Barra do Itapirapuã (BIT), Barra do Teixeira (BT), José Fernandes (JF), Mato Preto (MP), and Tunas (TU). High-resolution aeromagnetics (HRAM) and radiometric datasets were analyzed to assess the pattern of anomalies over the study area and then comparing these with previous studies.

GEOLOGICAL CONTEXT

Magmatic activity led to the emplacement of alkaline and alkaline-carbonatitic complexes in the South American Platform. This activity began in the Permian-Triassic and lasted until the Oligocene period while the majority of the complexes in Brazil are of Late Cretaceous age (Gomes and Comin-Chiaramonti 2005).

Alkaline province, according to Almeida (1983), is a term used to define areas of occurrence of clusters of alkaline bodies and are grouped mainly based on their geological setting and recognizable tectonic features (Gomes and Comin-Chiaramonti 2005, Riccomini *et al.* 2005). Although there is no clear consensus about the definition of alkaline rocks, they may be classified as igneous rocks, which are deficient in silica and/or alumina with respect to alkalis (Na_2O, K_2O, and CaO) and can vary from ultramafic to felsic (Fitton and Upton 1987).

The PGAAP resides in the PGA, which is an uplifted megastructure (Fig. 1) that extends for about 600 km in a northwest trend and hinge line dipping toward the inner part of the Paraná Basin (Piccirillo and Melfi 1988, Piccirillo *et al.* 1990). It comprises several northwest-trending tholeiitic dike swarms (Ussami *et al.* 1991, Renne *et al.* 1996, Brandt *et al.* 2009) and also four significant magnetic lineaments in the same direction (Fig. 1). The PGA is delimited by the Guapiara lineament in the northeast, by the Rio Piqueri lineament in the southeast while the arch's central region contains the São Jerônimo-Curiúva and Rio Alonzo lineaments (Raposo and Ernesto 1995).

Almeida (1983) pointed out thirteen intrusions for the PGA, namely: BN, BIT, Barra do Rio Ponta Grossa, BT, Cananéia, Itanhaém, IT, Jacupiranga, Juquiá, Mar Pequeno (Sabaúma, SP), MP, Sete Quedas, and Tunas. Later, two more bodies were added to this province: Pariquera-Açu and Registro (Ferreira and Algarte 1979, Ferreira *et al.* 1987, Mantovani *et al.* 2005). The ages of PGAAP occurrences are divided into two magmatic events, where one group is situated in the Early Cretaceous and the other in the Late Cretaceous (Gomes *et al.* 2011).

The igneous intrusions studied in this work (Tab. 1, Figs. 1 and 2) were chosen due to their grouped distribution in a rectangular area and the lack of magnetic and radiometric studies for them. The intrusions are presented in the geologic maps of Cerro Azul (Brumatti and Almeida 2014) and Apiaí (Morais *et al.* 2012). Geologic maps of the intrusions are illustrated in the Profile analysis section.

The Bairro da Cruz Complex is a small volcanic center with an area of approximately 1 km^2 showing an oval shape and irregular contours. It is comprised of coarse (olivine-gabbros) and fine (phonolites) varieties while its country rocks are mainly comprised of amphibole-schists and calc-silicate rocks (Hama *et al.* 1977). In addition, numerous small dikes (maximum of 1 m width) cut these gabbroic rocks in the area (Almeida 2016). K-Ar dating in pyroxene-amphibole resulted in an age of 230 ± 17 Ma for the Bairro da Cruz Complex (Hama *et al.* 1977). These authors suggest that this intrusion along the JF gabbro represents a previous basic-alkaline magmatism that occurred before the wide basaltic extrusion in the Paraná Basin.

The BN Complex alkaline intrusion has an area of approximately 8 km^2 (Gomes *et al.* 2018) and was emplaced into the Neoproterozoic Três Córregos granitic suite (Brumatti *et al.* 2015). Algarte (1972) and Kaefer and Algarte (1972) demonstrated that the intrusion is composed of nepheline syenites and phonolites while Brumatti *et al.* (2015) have divided the complex into five lithofacies: phlogopite melteigite, pink nepheline syenite, melanite-pseudoleucite-nepheline syenite, gray nepheline syenite, and sodalite syenite. The biotite Ar-Ar ages of BN range from 106 to 110 Ma (Gomes *et al.* 2018).

The IT Complex shows an NW-trending irregular shape and has an approximate outcropped area of 4 km^2 (Brumatti *et al.* 2015). This intrusion is emplaced into Cerro Azul Granite. Gomes (1970) reported that IT consists mainly of undersaturated medium to coarse syenitic rocks. Mafic syenites, melteigeites, and pulaskites occur in a less frequent distribution in the area while NW-trending decimeter tinguaite dikes crosscut the other alkaline petrographic types and the granitic country rocks (Gomes *et al.* 2018). IT is situated in an age interval of 102 and ~106 Ma, according to Ar-Ar determinations on biotite and U-Pb SHRIMP on titanite from melanitic syenitic rocks, respectively (Gomes *et al.* 2018).

The BIT Carbonatite is considered as a complex system (Loureiro and Tavares 1983) where there is an ellipsoidal network of dikes and veins of Fe, Mg, and Ca-carbonatites

Table 1. Summary of the main characteristics of the igneous rocks in the study area.

Rock name	Main lithotypes	Main classification	Coordinates	Age (Ma)	Carbonatites reported	REE reported
Bairro da Cruz Complex	Olivine-gabbros and phonolites	Alkaline, basic, intrusive/volcanic	24º52'S, 49º23'W	230 ± 17[a], Upper Triassic	No	No
Banhadão Complex	Nepheline syenites and phonolites	Alkaline, basic, intrusive	24º39'S, 49º23'W	106-110[b], Lower Cretaceous	No	No
Itapirapuã Nepheline syenite	Undersaturated syenites. Magnetite (south area)	Alkaline, basic, intrusive	24°41'27"S, 49°08'30"W	102-106[c], Lower Cretaceous	No	No
Barra do Itapirapuã Carbonatite	Carbonatites (plug)	Alkaline -carbonatite, intrusive	24°41'30"S, 49°13'00"W	129 ± 19[d], Lower Cretaceous	Yes (main rock and dikes)	Yes
Barra do Teixeira Phonolite	Peralkaline phonolites (plug)	Alkaline, basic, volcanic	49º26'S, 49º41'W	73-78[d,e], Upper Cretaceous	No	No
José Fernandes Gabbro	Variety of gabbros	Basic, intrusive	24°43'30"S, 48°58'59"W	134.93 ± 0.16[f], Lower Cretaceous	No	No
Mato Preto Complex	Nepheline syenites, phonolites, and carbonatites	Alkaline (carbonatites), basic, intrusive	24°45'S, 49°12'W	62-76[d,e] Paleocene to Upper Cretaceous	Yes (main rock and dikes)	Yes
Tunas Complex	Syenites and alkali syenites	Alkaline, felsic, intrusive	24°57'S, 49°06'W	70-85[d,g,h,i] Upper Cretaceous	No	No

[a] Hama *et al.* (1977), [b] Gomes *et al.* (2018), [c] Ruberti *et al.* (1997), [d] Cordani and Hasui (1968), [e] Sonoki and Garda (1988), [f] Almeida (2016), [g] Gomes *et al.* (1987), [h] Rugenski (2006), [i] Siga Jr. *et al.* (2007).

occupying an area around 2 km^2. This carbonatite is located inside the Ribeira Valley, being described as of difficult access and intense weathering (Loureiro and Tavares 1983). In addition to carbonatitic rocks, carbonatitic lamprophyric breccias and veins bearing quartz, fluorite, REE-rich apatite, REE fluorcarbonates, barite, and strontianite were found in the place (Ruberti *et al.* 2005). The age interpreted for the carbonatite is 129 ± 19 Ma, according to Ruberti *et al.* (1997), who used the Rb-Sr whole-rock technique.

The BT Phonolite represents a small circular body with 0.25 km^2 of area (Brumatti and Tomita 2014). Vasconcellos (1995) described the BT as composed of peralkaline phonolites hosting feldspar phenocrysts surrounded by fibro-radiated zeolites along with fluorite. It is considered a MgO poor small plug (Vasconcellos 1995, Vasconcellos and Gomes 1998). BT has an age of around 73–78 Ma, dating approximately to the end of the Cretaceous, according to K-Ar isotopic data (Cordani and Hasui 1968, Sonoki and Garda 1988).

The JF Gabbro is composed of gabbroic rocks, including cumulates, which are characterized by monzogabbros, layered gabbros, quartz monzogabbros and, to a lesser extent, monzonites (Almeida 2016). This suite is also intruded by synplutonic alkaline dikes (Almeida *et al.* 2019) and formed from batches of alkaline magma with different crustal contributions. Almeida (2016) dated an age of 134.93 ± 0.16 Ma (TIMS U-Pb zircon) for this complex.

The MP Complex, circular in shape and with 12 km^2 of area, is situated between the Neoproterozoic Três Córregos Granite and the Açungui Group. This intensely weathered suite (Loureiro and Tavares 1983) contains alkalic rocks (*e.g.* nepheline syenites, phonolites, porphyry phonolites, and tinguaites) which hosts ferruginous carbonatites and calciocarbonatites (Comin-Chiaramonti *et al.* 2001). There is also the existence of tuffs, agglomerates, and other silicate rocks, such as ijolites and melteigites. A variety of elements and minerals are related to the carbonatite suite in the MP complex, such as thorium, REE, iron, phosphorus, fluorite, magnetite, apatite, pyrite, bornite and in small amounts, uranium, niobium, titanium, and zirconium (Loureiro and Tavares 1983). Cordani and Hasui (1968), using K-Ar isotopic system, reported an age of approximately 66 Ma for a phonolite sample from MP while Sonoki and Garda (1988) outlined an age of 61.9 Ma and 76.4 Ma utilizing the K-Ar method, suggesting Late Cretaceous ages.

The Tunas Complex has an area of 22 km^2 in a NW direction (Brumatti *et al.* 2015). This plutonic structure with a felsic nature contemplates, in its majority, syenites and alkali syenites with subordinate alkali gabbros, syenogabbros, essexites, and syenodiorites (Gomes *et al.* 1987). Tunas contains 10% of volcanic breccias and small late dikes of syenitic composition (Ruberti *et al.* 2005, Marangoni and Mantovani 2013). The country rock consists of garnet-mica schists of Votuverava Group and schists and quartzites from the Perau Formation (Brumatti *et al.* 2015). The first ages for the massif were analyzed by Cordani and Hasui (1968) obtaining 110 Ma for two samples and 70 Ma for the others (K-Ar method), suggesting the possibility of this free-carbonatite intrusion having

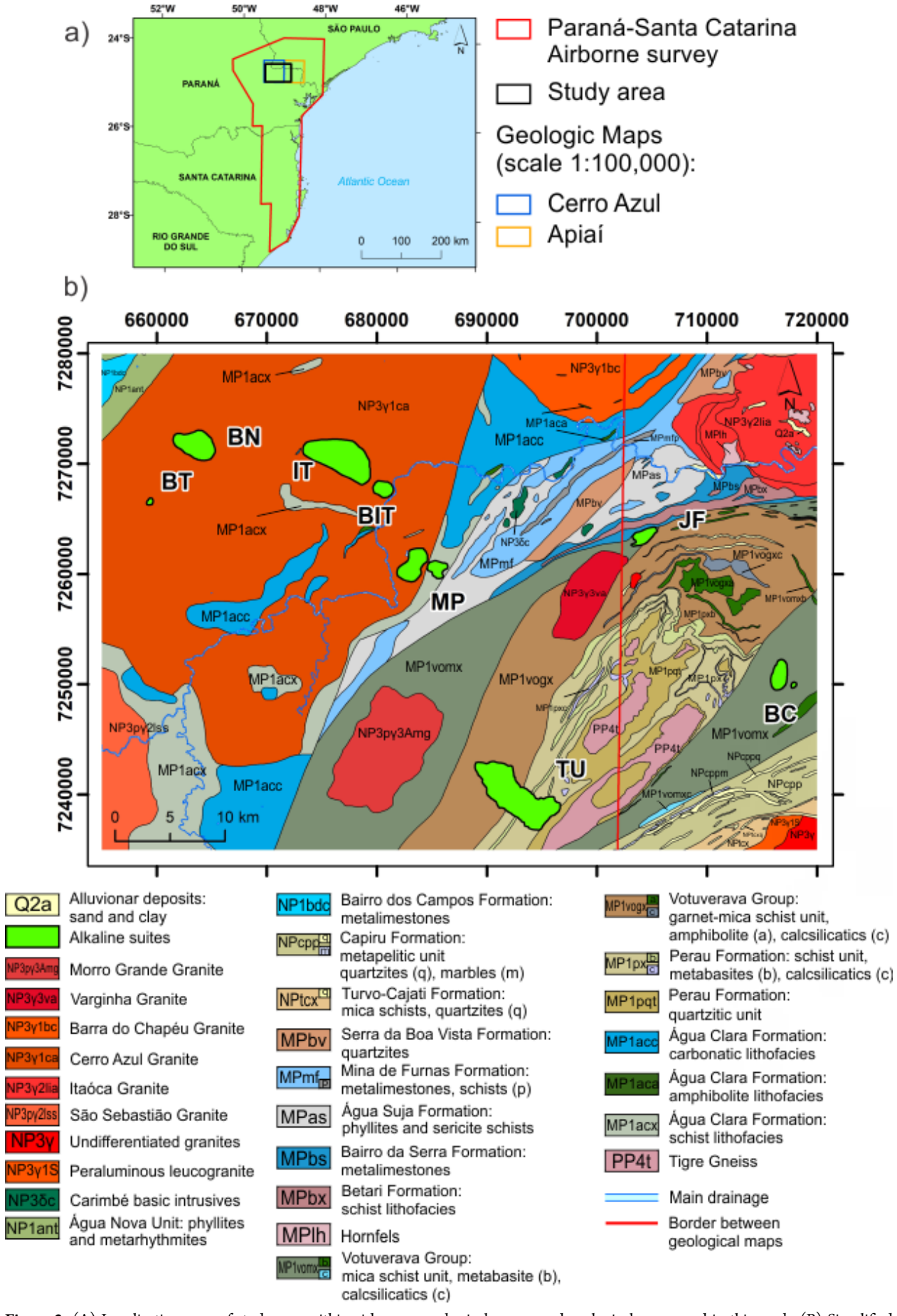

Figure 2. (A) Localization map of study area within airborne geophysical survey and geological maps used in this work. (B) Simplified geological map for the study area based on Cerro Azul (Brumatti and Almeida 2014) and Apiaí (Morais *et al.* 2012) maps. Alkaline complexes: Bairro da Cruz (BC), Barra do Itapirapuã (BIT), Banhadão (BN), Barra do Teixeira (BT), Itapirapuã (IT), José Fernandes (JF), Mato Preto (MP), and Tunas (TU).

generated in more than one magmatic activity. K-Ar age determination by Gomes *et al.* (1987) led to a mean value of 82 Ma. A similar age was determined by Rugenski (2006), 80.5 Ma, from Rb-Sr isotopic data. Siga Jr. *et al.* (2007) reported U-Pb syenite's zircon age dating for the Tunas complex around 83 Ma (ID-TIMS) and 85 Ma (SHRIMP).

MATERIALS AND METHODS

The study area was delimited by UTM zone 22S coordinates 655,000 – 720,000 and 7,280,000 – 7,230,000, comprising partial regions from the geological maps of Cerro Azul (Brumatti and Almeida 2014) and Apiaí (Morais *et al.* 2012) (Figs. 1 and 2). These 1:100,000-scale maps were used to discuss the geophysical data in association with the mapped geology.

Magnetic and gamma-ray spectrometric data were provided by the Geological Survey of Brazil (CPRM 2011) from the Paraná-Santa Catarina Project (PR-SC). This airborne survey was flown between 2009 and 2011, covering an area over 65,562 km^2 in the Paraná and Santa Catarina states, Brazil. North-south oriented flight lines were spaced 500 m apart. The data were acquired at a terrain clearance of 100 m. A Scintrex CS-3 high-sensitivity cesium vapor magnetometer sensor and Exploranium GR-820 airborne gamma spectrometer were used for data collection and the sampling rate for each sensor was 0.1 and 1 s, respectively. The coordinate system of the airborne survey was the World Geodetic System (WGS) 84 UTM Zone 22S and, therefore, all the geological and geophysical images created in this work adopted this coordinate system. All the magnetic and radiometric data were interpolated onto a 100 m grid cell-size, which represents 1/5 of the spacing between lines, using the minimum curvature algorithm (Briggs 1974, Swain 1976). All the gridding and magnetic and radiometric processing were performed in the Oasis Montaj suite.

The total magnetic anomaly (TMA), which is the difference between the measured and the geomagnetic fields (IGRF), was already corrected for the diurnal variations and microleveled by CPRM (2011). The data were then gridded and reduced to the pole (RTP, Baranov 1957, Baranov and Naudy 1964) according to the parameters calculated for the date of acquisition (Tab. 2). Moreover, the analytic signal of the vertical integral (ASVI) and the vertical integral of the analytic signal (VIAS) were gridded for use in 3D inversions. These techniques were introduced by Paine *et al.* (2001) and consist of transforming the TMA data into measures weakly dependent on the magnetization direction by calculating the total gradient of the vertical integration of the TMA or vertically integrating its total gradient. These quantities are treated as if they were reduced to the pole, allowing the 3D magnetic susceptibility algorithm inversion developed by Li and Oldenburg (1996) to be performed. Li *et al.* (2010) pointed out that the data transformed by this method are not true magnetic anomalies while the inversion algorithm used considers only induced magnetization. Although there is this inconsistency, both ASVI and VIAS lead to interpretable results (Leão-Santos *et al.* 2015, Li 2017), being appropriate for isolated or multiple sources as well (Pilkington and Beiki 2013).

The complexes that showed a significant magnetic response, *i.e.* Bairro da Cruz, JF, and Tunas, were 3D unconstrained inverse modeled to obtain an estimate of the distribution of their magnetic susceptibilities and emplacement depth. Inversions were applied in the TMA, VIAS-TMA, and ASVI-TMA grids. The RTP parameters for each modeled body were described in Table 2, while the parameters used for the inversions in the Oasis Montaj suite were illustrated in Supplementary Material A. RTP processing assumes that remanent magnetization is parallel to the current inducing field direction (Li *et al.* 2007), and it may introduce additional artifacts into the data. This technique can make the inversion algorithms ineffective, which was our case, where a significant number of small bodies (artifacts) were created, and, therefore, we decided not to represent this model in this work.

In terms of radiometric processing, basic grids (K, eTh, and eU) were corrected following the procedure of Ferreira *et al.* (2009) where each radioactive element received a constant to keep its minimum value to 0.01 and, therefore, avoiding divisions by values equal to or below zero when ratioing. The constants added to the K, eTh, and eU grids were 1.05%, 1.22 ppm, and 2.39 ppm, respectively. A ternary R-K, G-eTh, B-eU image was also generated for the study area. Fourteen ratio maps were created following the procedure of Grant (1998), where instead of calculating the ratios from line data and then gridding them, divisions were performed from the gridded data. The ratios generated were: K/eU, K/eTh, K/(eU + eTh), F = K*(eTh/eU) (F-parameter, Efimov 1978, Gnojek and Prichystal 1985), eU/eTh, eU/K, eU/(K + eTh), eU/(K + eU + eTh), eTh/K, eTh/(K + eU), (eTh + eU)/K, (K*K)/(eU*eTh), (eU*eU)/eTh, and (eTh*eTh)/K. In addition, the parameters thorium-normalized potassium (KD), thorium-normalized uranium (UD), and DRAD, *i.e.* UD-KD (Saunders *et al.* 1987, 1993, 1994) were also implemented to evaluate the concentration of potassium and equivalent uranium when they are normalized in relation to eTh. Equal-area distribution was used for zone color ranges in the analysis of ratios and other parameters images.

The minimum, mean, and maximum levels of K, eTh, and eU of each intrusion in the study area were determined from the gridded data and plotted in box-plot charts. A note of

Table 2. Parameters used for the reduction to the pole for the study area and inverse modeled igneous rocks in this study.

Region	Magnetic inclination	Magnetic declination	Amplitude correction inclination
Study area	-34.49	-18.91	-55.51
Bairro da Cruz	-34.96	-19.02	-55.04
José Fernandes	-34.73	-18.79	-55.27
Tunas	-34.87	-18.86	-55.13

caution is due here since our radiometric interpretation was done using the standard units for each radioelement channel, *i.e.* % for K and ppm for eU and eTh, with an emphasis in aiming possible exploratory targets from the radioactive distribution and does not necessarily report the absolute values of K, eU, and eTh. For example, the potassium data was not transformed in ppm since it would overwhelm the contribution of equivalent thorium and uranium channels. Also, radioelements concentrations for each sampled data point inside complexes' boundaries (according to the geological maps previously described in this work) were illustrated in normalized ternary diagrams created in the TriPlot software and later refined in the Origin suite to identify trends in K, eTh, and eU concentrations. Negative sampled data points were assigned null values to avoid miscalculating relative concentrations of K, eTh, and eU in the diagrams.

Stacked profiles containing the variables K, eU, eTh, TMA, RTP-TMA, and Digital Terrain Model (DTM) from the PR-SC airborne survey flight lines were plotted along the mapped lithotypes for each intrusion to assess their absolute and relative levels. Profiles are useful to display more reliable data, *i.e.* with full spatial resolution, than a grid. This is due to the use of filters along flight lines for the grid interpolation to avoid aliasing problems (Horsfall 1997). No correction of negative or zero values for the radioelements was applied. This derives from the fact that quantities below or equal to zero may be a valid representation of the radiometric dataset, which is characterized by statistics and, therefore, supports data that lie outside the expected interval of values, even after all the treatments carried after the acquisition phase (Grant 1998).

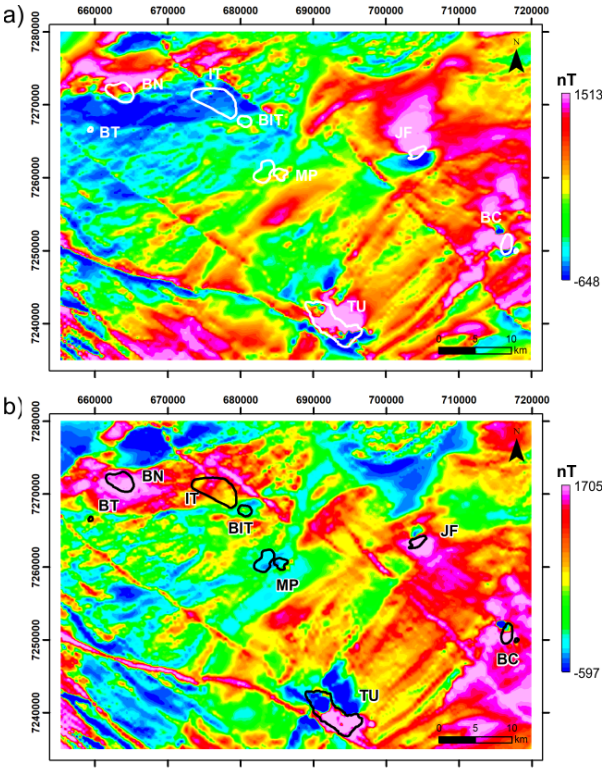

Figure 3. (A) TMA map data from study area and (B) its reduction to the pole. (A) Thick white and (B) black lines represent the alkaline complexes: Bairro da Cruz (BC), Barra do Itapirapuã (BIT), Banhadão (BN), Barra do Teixeira (BT), Itapirapuã (IT), José Fernandes (JF), Mato Preto (MP), and Tunas (TU).

RESULTS AND DISCUSSION

Magnetic anomaly of the study area

Total magnetic anomaly values presented an interval of approximately 1,000 nT (Fig. 3). No significant representation of classical dipolar anomalies was observed for IT, BIT, BN, BT, and MP igneous rocks even when TMA data were interpolated in a rectangular area around the location of the intrusions. This behavior can be explained by the common lack of strong magnetization of these rock types (Airo 2015). For example, some alkaline complexes in the Goiás Alkaline Province, such as Diorama, Morro do Macaco, and Amorinópolis (Dutra *et al.* 2012, Marangoni and Mantovani 2013) did not show a specific magnetic signature. It should be noted that the BIT and the MP complexes did not produce circular magnetic anomalies or any distinctive magnetic signature, unlike other alkalic-carbonatitic complexes cited in the literature (*e.g.* IIvaara, Sokli, Airo 2015).

The dipolar anomaly of Bairro da Cruz Complex could be attributed to the presence of coarse olivine-gabbros (Hama *et al.* 1977), which is one of the most ferromagnetic igneous rocks (Clark 1999). The same could be said for the JF Gabbro, an intrusion with a strong magnetic response that was even detected in lower quality airborne survey datasets (Ferreira and Algarte 1979).

Higher anomalies are located in the eastern part of the study area and to a lesser extent in its southeast and in the north of the BN and IT suites. The shape and NW direction of the anomalies in the southwestern part (Fig. 3B) infer that the magnetic source bodies are comprised of dikes. Dike swarms are widely presented in the PGA (Raposo and Ernesto 1995, Brumatti and Almeida 2014).

Inversions

The intrusions that presented a significant magnetic response were inversely modeled to assess their magnetic susceptibilities and depths (Figs. 4 and 5 for Bairro da Cruz, Figs. 6 and 7 for JF, and Figs. 8 and 9 for Tunas). TMA, ASVI-TMA, and VIAS-TMA grids for Bairro da Cruz, JF, and Tunas were illustrated to compare the magnetic susceptibility model with each grid. It is known that diabase dikes in the area can carry remanence and therefore could influence the response for the igneous bodies. However, Raposo and Ernesto (1995) demonstrated that the vast majority of dikes in the PGA have remanent magnetization with normal polarity. Furthermore, TMA grids of Bairro da Cruz (Fig. 4A), JF (Fig. 6A), and Tunas (Fig. 8A) showed positive anomalies in their north lobes while negatives ones concentrated over their southern portions. This is in good agreement with induced magnetic responses for bodies located in the earth's southern hemisphere that are not significantly affected by remanence (Louro *et al.* 2017). All inversions are

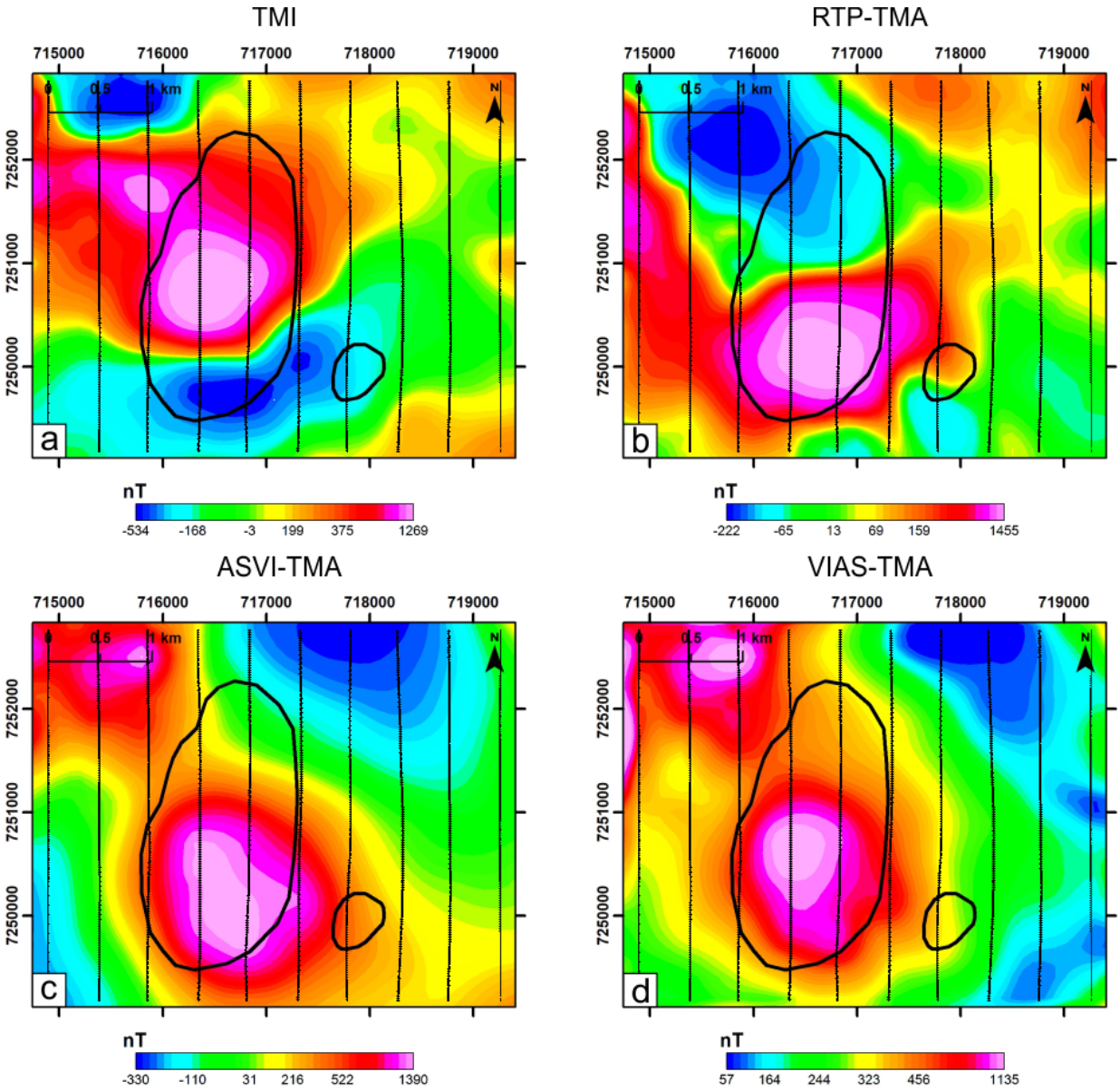

Figure 4. Magnetic responses of Bairro da Cruz Complex (black polygons): (A) Total magnetic anomaly (TMA), (B) TMA reduced-to-pole (RTP-TMA), (C) Analytic signal of the vertical integral of TMA (ASVI-TMA), (D) Vertical integral of the analytic signal of TMA (VIAS-TMA). N-S oriented black lines are the airborne survey flight lines.

illustrated in detail in Supplementary Material B, which consists of 3D PDF files.

Bairro da Cruz Complex

It is known from the literature that TMA airborne magnetic data for BC are situated between -250 and 500 nT (Ferreira and Algarte 1979) and configure a normal dipole anomaly (Almeida 2016). Figure 4A illustrates magnetic values around -530 nT for the negative lobe of BC anomaly and over 1,260 nT in the positive one. This represents an increase of over two times in the amplitude interval reported by Ferreira and Algarte (1979). It may be reasonable to suppose that the lower values found for BC are due to the lower data quality of the airborne survey acquired (CPRM 1978), which consisted of space between flight lines of 1 km and flight height of 150 m.

The reduced to the pole anomaly was not located in the center of the outcropped Bairro da Cruz borders (Fig. 4B). Better results were found for the ASVI and VIAS of TMA data (Figs. 4C and 4D). No significant differences were found between these two methods. Moreover, none of the grids resulted in an appropriate response for the eastern body of Bairro da Cruz. All the enhancement methods applied practically showed scarce differences in this area. A possible explanation for this might be that this complex has a different composition than its western counterpart and, therefore, lacks any magnetic contrast to its country rock. It is important to bear in mind that in the geological map presented by Hama *et al.* (1977), there is no eastern part for the Bairro da Cruz intrusion while the Apiaí geologic map (Morais *et al.* 2012) lacks any information about this mapped rock related to its petrography or composition.

Inversions revealed that the contrasts of apparent magnetic susceptibility were similar (Fig. 5). The TMA model created several bodies and no significant correlation was

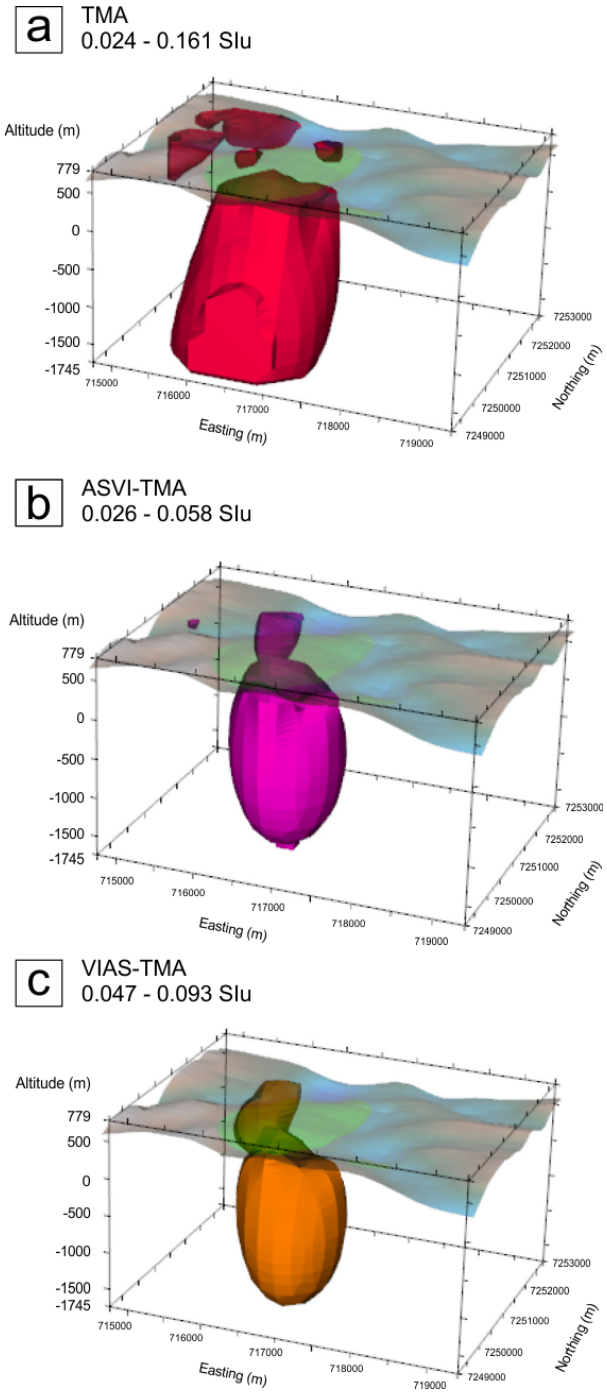

Figure 5. Contrast of apparent magnetic susceptibility distribution in 3D models for each type of Bairro da Cruz gridded data described in Figure 4 (except for the RTP-TMA grid). Models were cut in an arbitrary threshold value (displayed on the image) to create a better representation of the surface geology. Minimum values for each model: -0.111 (TMA), -0.046 (ASVI-TMA), and -0.058 SIu (VIAS-TMA). The maximum values of magnetic susceptibility were not modified. Altitudes are GPS altitudes and zero values correspond to the Mean Sea Level (MSL). The blue and brown colored grid over the top represents the Digital Terrain Model (DTM) for the area, which ranges from 795 to 279 m. The green polygon in this grid represents the Bairro da Cruz geologic surface boundaries.

found with the outcropped surface. The ASVI-TMA and VIAS-TMA inversions displayed ellipse-shaped features with magnetic susceptibility distribution more elongated in the depth axis. All the models have illustrated susceptibilities inside the range for gabbros, *i.e.* 3.10^{-4} to 3.10^{-1} SIu (Clark 1997). Negative values of magnetic susceptibility were situated above -1, which can be explained by diamagnetic minerals (*e.g.* quartz) in the meta-arenites and quartzites present in the country rock of Bairro da Cruz, Mica schists unit. However, phonolite magnetic susceptibilities (10^{-5} to 10^{-3} SIu, Clark 1997) were not successfully represented in the modeling of Figure 5. One possible explanation for this is that the Bairro da Cruz is a small body and, therefore, it could not be appropriately sampled in the airborne survey. Another reason is that the phonolites are weakly magnetic (Clark and Emerson 1991), thus ensuring a poor distribution of magnetic susceptibility for this rock type.

Altitudes for all the susceptibility models were situated between 750 and -1,750 m. In summary, these results suggest that the Bairro da Cruz could have a thickness of around 2.5 km, reaching a depth of more than 1.5 km below the Mean Sea Level.

José Fernandes Gabbro

It can be seen that a magnetic dipole with normal polarity is presented for the JF Gabbro (Fig. 6A). This result reflects those of Ferreira and Algarte (1979) and Almeida (2016), who also found a similar anomaly for this body. The RTP data (Fig. 6B) displayed amplitudes around 1,600 nT while it has positioned the center of the anomaly in the western portion of the geological body while the ASVI-TMA and VIAS-TMA (Figs. 6C and D) created two strong anomalies located near the center of the gabbro. None of the models displayed anomalies with the same NE-trend observed for the outcropped gabbro.

The magnetic susceptibility inversion models (Fig. 7) illustrated values between 0 and 0.220 Slu, which is consistent with gabbros results from Clark (1997). JF is emplaced in metasedimentary rocks (Morais *et al.* 2012) and, thus, values of susceptibility below or close to zero could be attributed to those rock types. The models were situated between 750 and -1,500 m of altitude, thus, suggesting thickness for the causative sources of around 2,000 m. A note of caution is due here since there is no magnetic data available which could support better approximations for the distribution of susceptibility.

Tunas Complex

It can be observed from the total magnetic anomaly data (Fig. 8A) that positive values in the north and low values in the south of the area may correspond to the mapped Tunas geology. However, it is in the southeastern portion of this alkaline complex that a dipole anomaly with more than 1 km of extension could be visualized. TMA values were situated in the -650 and 1,510 nT interval, which are higher than those reported by Ferreira and Algarte (1979) and Rugenski (2006), *i.e.* -600 to 1,000 nT, and -300 to 800 nT, respectively. A possible explanation for this might be that these authors have processed data from the Serra do Mar airborne survey (CPRM 1978), which has different flight lines directions (*i.e.* NW) and is undersampled comparing to the PR-SC project. RTP, ASVI, and VIAS applied to the TMA data (Figs. 8B, 8C and 8D) have positioned a strong anomaly over the southeastern area of Tunas massif with maximum values around 1,600 nT

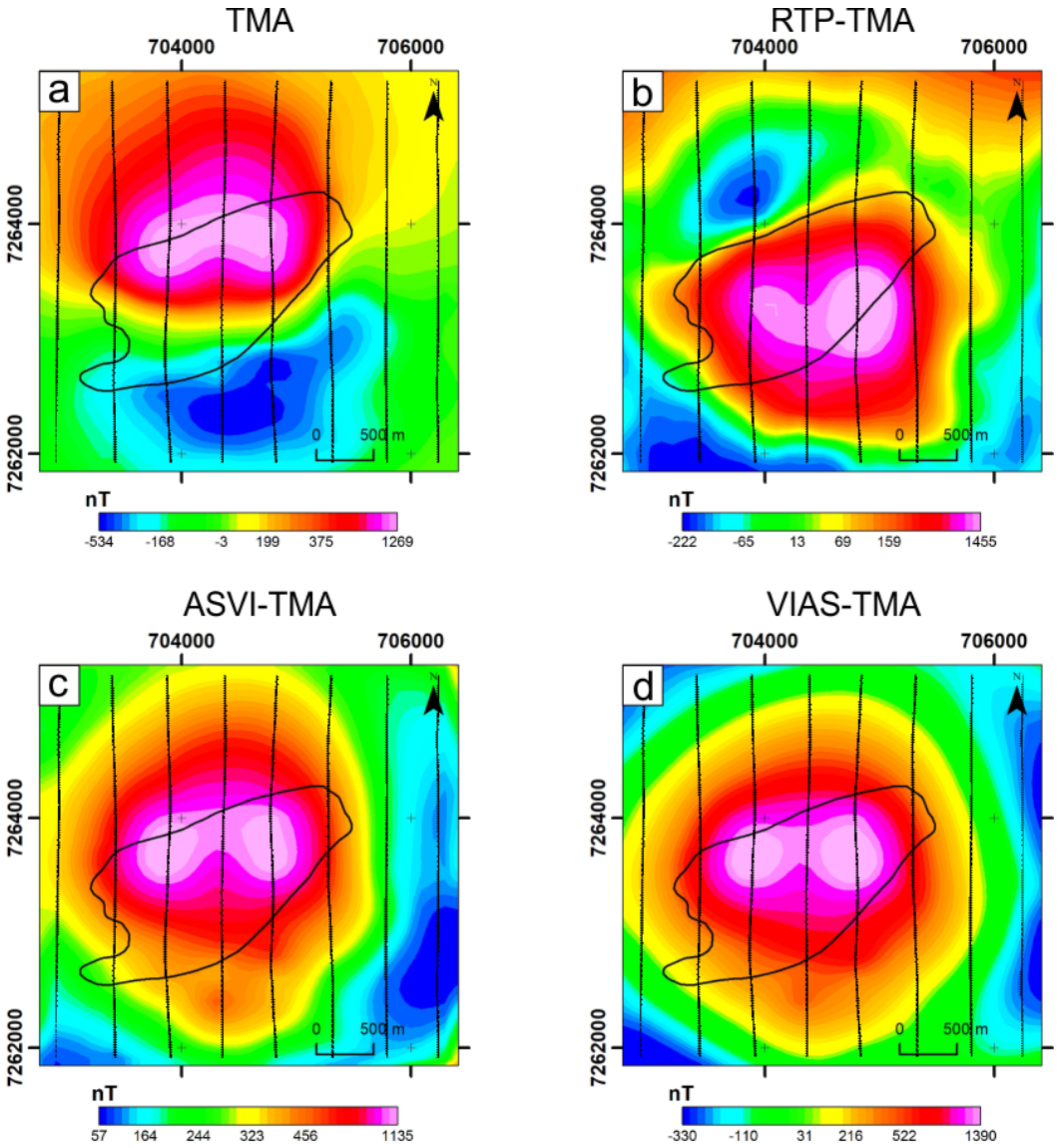

Figure 6. Magnetic responses of José Fernandes Gabbro (black polygon): (A) Total magnetic anomaly (TMA), (B) TMA reduced-to-pole (RTP-TMA), (C) Analytic signal of the vertical integral of TMA (ASVI-TMA) and (D) Vertical integral of the analytic signal of TMA (VIAS-TMA). N-S oriented black lines are the airborne survey flight lines.

and up to 3,000 nT for the VIAS-TMA image (Fig. 8D). This result may be explained by the fact that the VIAS technique may cause significant amplification of low-frequency components of the data, which is a drawback of this method pointed out by Paine *et al.* (2001).

Distribution models of contrast of apparent magnetic susceptibility (Fig. 9) demonstrated an NW-trend. This finding is consistent with that of Brumatti *et al.* (2015), who mapped Tunas. However, our results were not very encouraging since they created a significant quantity of bodies for the TMA data, while ASVI and VIAS enhancements do not correspond to the outcropped geology of a single intrusion. The values ranged between 0.02 and 0.25 SIu. Comparison of these results with those of other studies related to other alkaline complexes in Brazil suggest similarities, such as Jacupiranga (0.001 to 0.161 SIu, Alva-Valdivia and López-Loera 2011), Juquiá (0.048 SIu, Rugenski 2006), Araxá (maximum of 0.234 SIu, Pereira *et al.* 2010), and Catalão I (0.17 SIu, Mantovani *et al.* 2016).

The largest axis of Tunas models had 6,000 m while its minor one had 2,500 m. The contrast of apparent magnetic susceptibility models had altitudes between 1,000 and -2,500 m. This result is similar to that of Rugenski (2006), who reported a depth of around 3,000 m for the bottom of this body using 2.5D modeling.

Radiometric analysis

Figure 10 provides an overview of K (%), eTh (ppm), and eU (ppm) concentrations for each intrusion according to the data of the PR-SC project. What stands out in the box-plot charts is that eTh is the most abundant radioactive element for all suites, sometimes extrapolating values of 50 ppm. In addition, practically all the minimum, maximum, and mean quantities of eU are higher than K ones. This radioelement has its highest concentration in the MP suite (5.07 %). Also, this intrusion has the highest average of potassium values (2.27 %). Overall, eU and K have lower concentrations in comparison with eTh. For example, there is a 20-fold increase

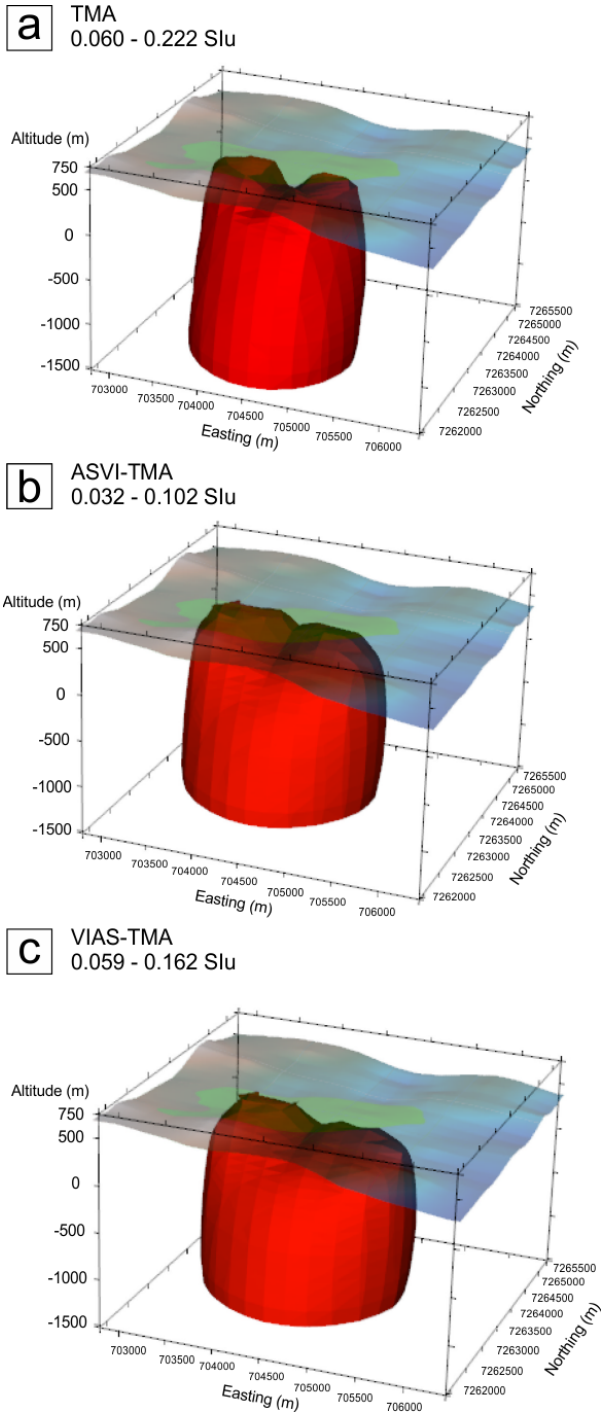

Figure 7. Contrast of apparent magnetic susceptibility distribution in 3D models for each type of José Fernandes gridded data described in Figure 6 (except for the RTP-TMA grid). Models were cut in an arbitrary threshold value (displayed on the image) to create a better representation of the surface geology. Minimum values for each model: -0.108 (TMA), -0.039 (ASVI-TMA), and -0.074 SIu (VIAS-TMA). The maximum values of magnetic susceptibility were not modified. Altitudes are GPS altitudes and zero values correspond to the Mean Sea Level (MSL). The blue and brown colored grid over the top represents the Digital Terrain Model (DTM) for the area, which ranges from 717 to 320 m. The green polygon in this grid represents the José Fernandes Gabbro geologic surface boundaries..

in this radioelement averaged concentration compared to eU in the BIT Carbonatite. In addition, this intrusion displayed mean concentrations of K, eU, and eTh as follows: 0.54 %, 24.37 ppm, and 413.24 ppm, respectively. The higher values for eTh and eU, in particular eTh, support evidence from previous studies (Ford *et al.* 1988, Verplanck and Gosen 2011), which demonstrated that high values of both elements, especially eTh, are frequent in carbonatites and REE-bearing alkaline intrusions. For instance, Ford *et al.* (1988) reported values for the Allan Lake carbonatite (Canada), ranging from 1.4–3.5 %, 0.5–3.8 ppm, and 14.5–119.4 ppm for K, eU, and eTh, respectively. Similarly, the MP Complex has K concentrations situated in intervals of 0.08 to 5.07 %, eU in 2.43–27.23 ppm, and eTh in 21.76–443.49 ppm. This alkalic-carbonatitic suite showed the highest values of eTh, except for BIT. A possible suggestion for this is that while BIT is comprised in its majority of carbonatites, and thus frequent displaying large eTh values, MP has alkaline lithotypes in its configuration, lowering the average concentrations for that radioelement.

Overall, whereas K and eU levels for the complexes studied in this work were consistent with one of the rock types defined by Killeen (1979) or Galbraith and Saunders (1983), eTh for the same complex demonstrated to be higher than the average for these authors' classification. That is, the bodies showed some discrepancy for both classification systems at least in one radioelement. These findings may somewhat limit the creation of a generic system to characterize each complex. This is due to the fact that they are composed of different alkaline lithofacies in the majority of the cases and, therefore, display different radioelements levels according to their lithofacies composition.

Table 3 displays the responses for radiometric ratios and parameters previously stated in this work. The responses were based on relative values of the intrusions around each of their country rock according to the images for each parameter presented in Supplementary material C. Pink to red colors in the gridded images were attributed to high values, the majority of yellow and green colors were considered medium values and blue color was considered low. It can be seen that high concentrations of eTh and eU are presented for BN, IT, BIT, MP, and Tunas complexes while the other bodies have displayed medium to low values for these radioelements. MP is the only one of the complexes studied that revealed higher potassium values. However, the KD for this body displayed low responses, suggesting that soil and/or vegetation may have influenced concentrations of K.

F-parameter alongside ratios with K variable in the numerator showed responses that lack any pattern to characterize alkaline complexes and gabbros. Overall, these parameters presented low to medium values but do not show a significant correlation for the bodies in the study area.

Ratios with eU term in numerator revealed high responses in general. eU/K and (eU^2)/eTh ratios allowed to differentiate between the gabbros (BC and JF) and the other alkaline complexes. The responses for the alkalic rocks are high whereas the gabbros showed medium to low values. No significant pattern was found in UD and DRAD parameters that would allow a clear distinction between the bodies.

Equivalent thorium term in numerator ratios showed high responses for all the bodies, except Bairro da Cruz, BT, and JF, which displayed medium to low values. This is coherent

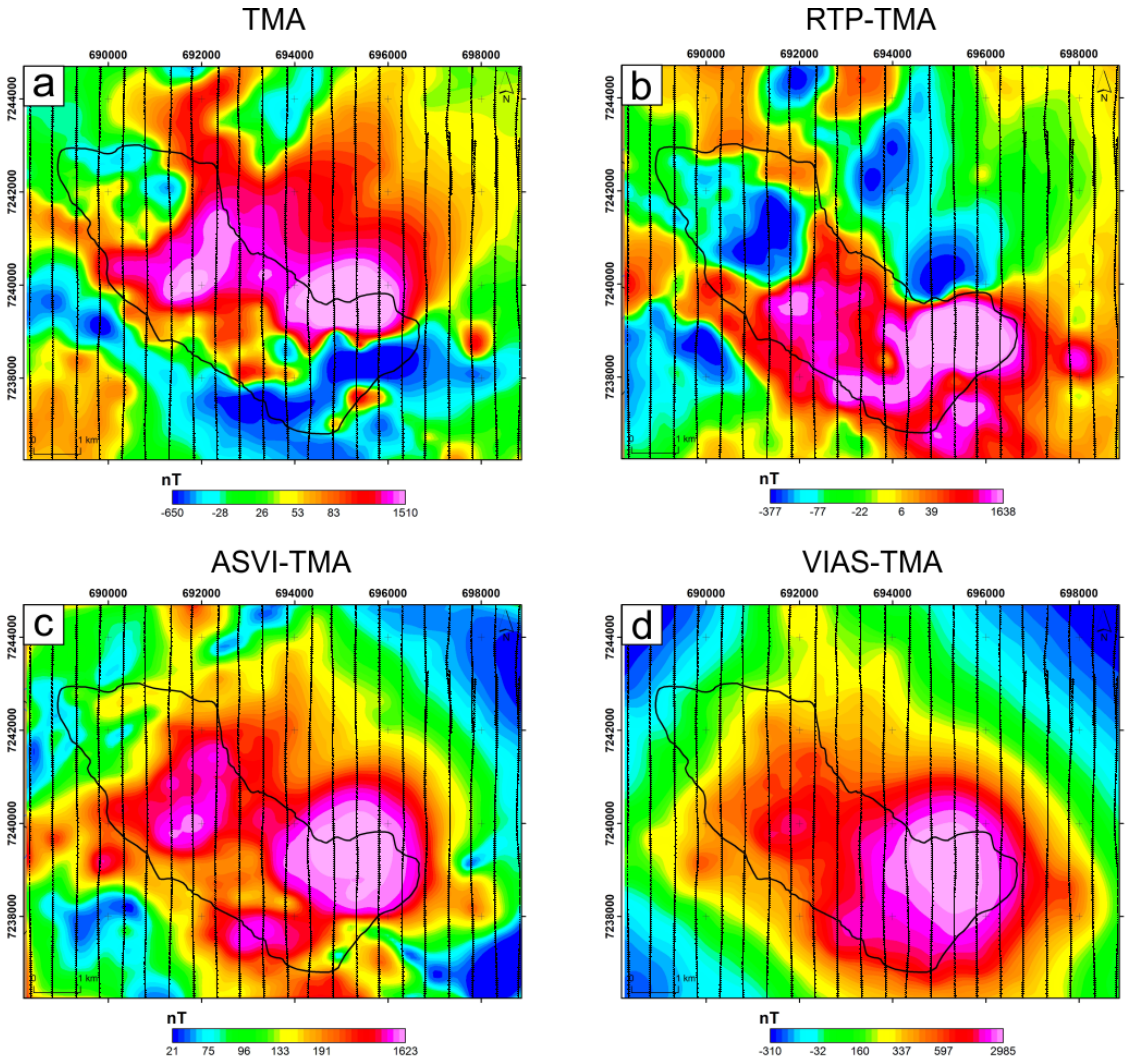

Figure 8. Magnetic responses of Tunas Complex (black polygon): (A) total magnetic anomaly (TMA), (B) TMA reduced-to-pole (RTP-TMA), (C) Analytic signal of the vertical integral of TMA (ASVI-TMA) and (D) Vertical integral of the analytic signal of TMA (VIAS-TMA). N-S oriented black lines are the airborne survey flight lines.

with previous findings from this work where eTh is the most abundant element for all the igneous suites.

RGB colors for each suite comprised cyan and black overall. The cyan color suggests that eU and eTh are presented in the rock while there is some lack of potassium. Black color indicates the absence of radioelements. Only the MP suite displayed higher values for all radioactive elements.

Figure 11 reveals ternary diagrams of relative (normalized to 100 %) K, eTh, and eU concentrations for each sampled data point of the complexes studied in this work. All the igneous rocks have relative quantities of eTh above 60 % with the majority of sampled points situated between 70 and 90 %. Almost none of the complexes reached 20 % K concentrations, except Bairro da Cruz, which has few points above this threshold. The majority of intrusions were situated between 0 and 25 % of eU relative concentrations while IT is the unique body to reach levels around 40 %. It is worth noting that this intrusion, unlike its neighbors, has its sampled data grouped along the eTh edge. The IT Complex showed a distribution with almost 100 % of eTh and decreased along this edge to 60 % while eU increased in the opposite direction and K percentages remained relatively stable. BIT, on the other hand, demonstrated a higher data density with 62 points situated around 0 to 1 % of K and 90 to 100 % of eTh.

Profile analysis

For this section, profiles along flight lines for each igneous suite were displayed showing the K, eTh, eU, TMA, RTP-TMA, and DTM responses in the N-S direction.

Bairro da Cruz Complex

It can be seen that the radioelements levels from the Mica schists unit (Morais *et al.* 2012) start decreasing (K and eU) or remain stable (eTh) when entering the BC Complex (Fig. 12). In this igneous intrusion, K and eTh increased its concentrations toward the body's central part. For the latter, its figure reached around 7 ppm when there was also a maximum of K concentration (*i.e.* 1.7 %) and remained constant until drops to over 5 ppm after 500 m approximately. Equivalent uranium has displayed some high and low peaks, but, in general,

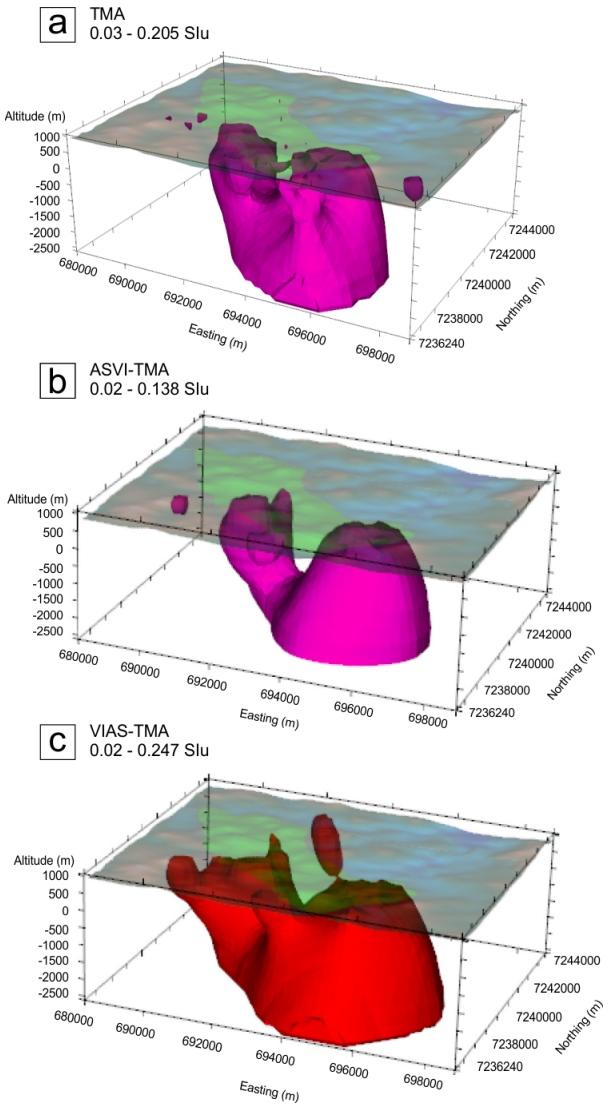

Figure 9. Contrast of apparent magnetic susceptibility distribution in 3D models for each type of Tunas Complex gridded data described in Figure 8 (except for the RTP-TMA grid). Models were cut in an arbitrary threshold value (displayed on the image) to create a better representation with of surface geology. Minimum values for each model: -0.088 (TMA), -0.05 (ASVI-TMA), and -0.079 SIu (VIAS-TMA). The maximum values of magnetic susceptibility were not modified. Altitudes are GPS altitudes and zero values correspond to the Mean Sea Level (MSL). The blue and brown colored grid over the top represents the Digital Terrain Model (DTM) for the area, which ranges from 1,049 to 681 m. The green polygon in this grid represents the Tunas Complex geologic surface boundaries.

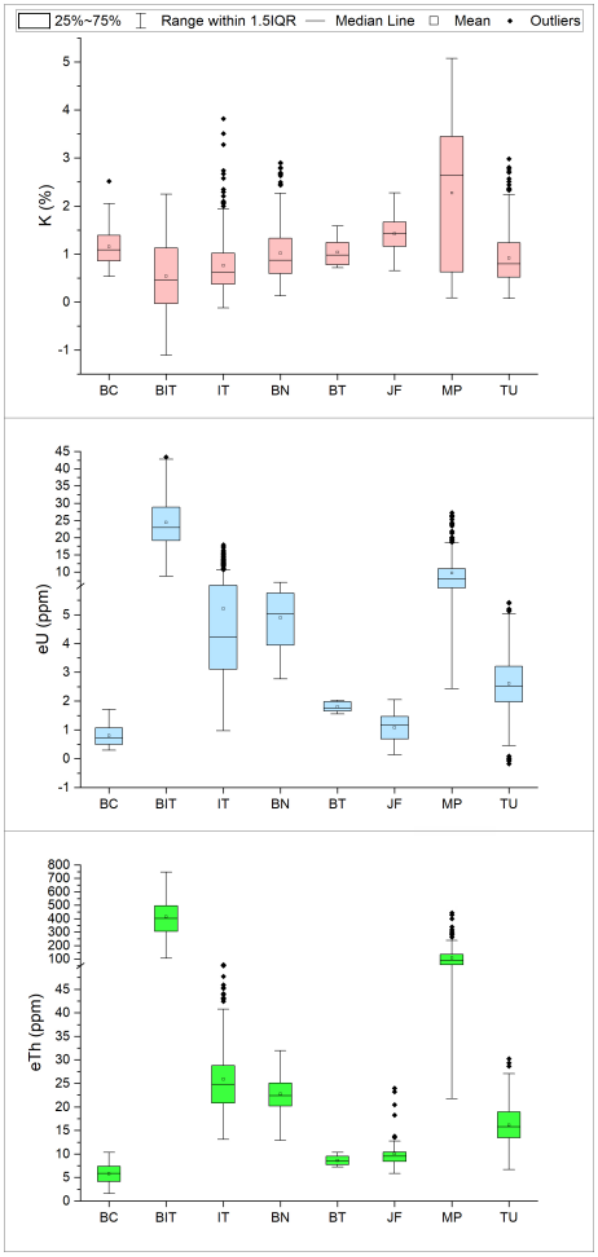

Figure 10. Box-and-whisker plots of radiometric data from the airborne geophysical survey. IQR stands for interquartile range. Alkaline complexes: Bairro da Cruz (BC), Barra do Itapirapuã (BIT), Banhadão (BN), Barra do Teixeira (BT), Itapirapuã (IT), José Fernandes (JF), Mato Preto (MP), and Tunas (TU). Note that the eU and eTh plots have a scale break to improve readability since there are large differences between the high and low values of the data.

remained virtually stable. In the central part, where eTh kept constant, that radioelement reached its lowest values inside the igneous suite.

Total magnetic anomaly values revealed the lowest values in the south area of Bairro da Cruz (Fig. 12), reaching -400 nT and maximum (over 500 nT) in the central part of the profile. TMA slightly diminishes to 100 nT northward along the profile. RTP-TMA results showed some good correlation positioning the TMA anomaly over the central area, although it has located the anomaly further to the southern part of Bairro da Cruz. It is important to highlight the fact this intrusion may have not been mapped in the literature using a fine-detail scale, and thus, our results suggest that BC geological contacts may be extended in the southern direction, where the RTP-TMA is positioned.

Banhadão Complex

The profile data for BN Complex can be visualized in Figure 13. Potassium distribution has displayed levels between 0.6 and 2.2 %. The highest concentration of this radioelement is located between the Phlogopite melteigeite (Kλbam) and Pink nepheline syenite (Kλbansr) units in the central part of BN. The Sodalite syenite (Kλbass) unit showed the lowest values for K, eTh, and eU with 0.6 %, 18, and 4 ppm, respectively.

Table 3. Gamma-ray spectrometric and magnetic responses of igneous rocks in the study area. The blue stands for relatively low values while yellow and red are for medium and high values, respectively. The letter D in the TMA row represents that the body showed a dipole anomaly response. Igneous rocks: Bairro da Cruz (BC), Barra do Itapirapuã (BIT), Banhadão (BN), Barra do Teixeira (BT), Itapirapuã (IT), José Fernandes (JF), Mato Preto (MP), and Tunas (TU).

	Igneous rocks							
Variable	**BC**	**BN**	**IT**	**BIT**	**BT**	**JF**	**MP**	**TU**
K								
eTh								
eU								
K/eTh								
K/eU								
K/(eU+eTh)								
(K^2)/(eU*eTh)								
F=K*(eU/eTh)								
eU/K								
eU/(K+eTh)								
eU/(K+eU+eTh)								
eU/eTh								
(eU^2)/eTh								
eTh/K								
(eTh^2)/K								
(eTh+eU)/K								
eTh/(K+eU)								
Kd								
Ud								
DRAD								
Color in RGB	Black	Cyan	Cyan	Cyan	Black	Black	White	Cyan
TMA		D				D		D

Equivalent uranium values in the BN Complex increased gradually from its southern part, peaking between the Gray nepheline syenite (Kλbansc) and Pink nepheline syenite (Kλbansr) geological contact and then slowly decreasing until the Sodalite syenite (Kλbass) lithofacies. The figure for eTh is somewhat similar to the eU one, although it is more erratic with sharper increases and decreases at some points over the profile.

TMA and RTP-TMA values slightly increased from south to north of the BN Complex, showing negative values in the Gray nepheline syenite (Kλbansc) unit and slowly went up to 100 nT in the northernmost part of the profile inside the BN suite. The lack of any highs or lows between the lithofacies suggests that there is no significant contrast of magnetic susceptibility in this intrusion.

Itapirapuã Nepheline syenite

Figure 14 provides an overview of the radioelement concentrations and TMA data in the flight line 12035:677 which has flown in the IT syenite. Ranging intervals for this intrusion are: 0–3.75 % K, 20–37 ppm eTh, and 2–14 ppm eU. What is interesting about the data in this profile is that all radioelements have peaked at virtually the same Y-coordinate (eTh peaked some meters near the south of this coordinate), located in the center of the IT Nepheline syenite. In addition, a local low near the northern part of the peak described above is observed for K, eTh, and eU, then followed northward by a local high.

Along the N-S profile (Fig. 14), the magnetic data displayed negative levels. The figures for the IT Nepheline syenite are around -100 nT (minimum) and -50 nT (maximum). The small difference between the maximum and minimum values indicates that there is a paucity of major contrast of magnetic susceptibility over this intrusion. In addition, the magnetic response appeared to be unaffected by the Fe mineralization near the profile.

Barra do Itapirapuã Carbonatite

This carbonatite body displayed higher concentrations of eU and eTh than its country rock (Fig. 15), *i.e.* Cerro Azul Granite. The maximum values of these radioelements for this intrusion are 45 ppm eU and 550 ppm eTh and are located in the southernmost part of the BIT profile. These values then steadily drop toward the north of the profile. On the other hand, the opposite occurs for the potassium data. Its distribution starts decreasing when entering in the southern portion of the BIT, reaches a small increase of around 1.0 % and then plunge to near zero to start rising near the contact with Cerro Azul Granite. Then, this figure remains almost constant until rising above 3.0 % at the end of the profile.

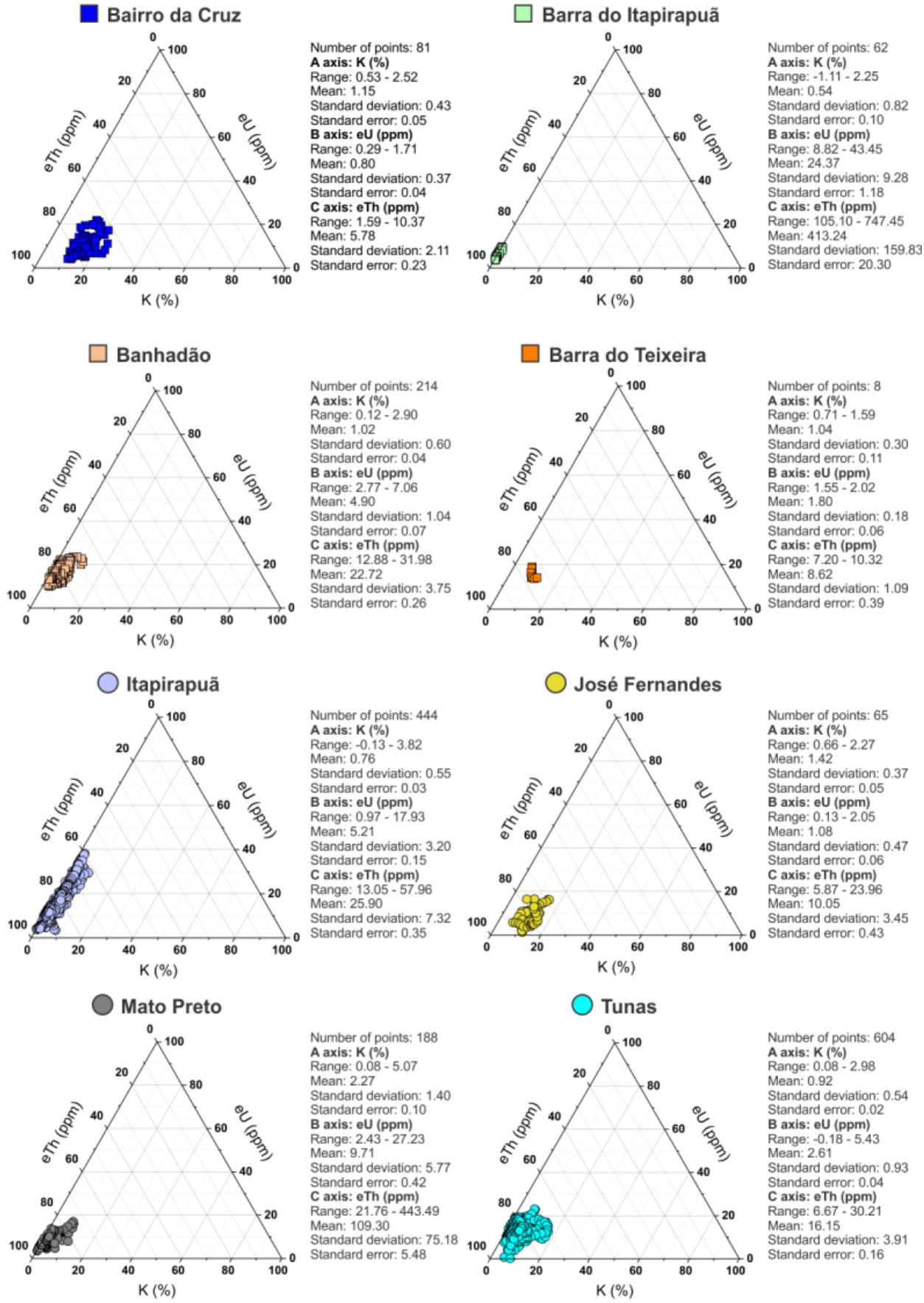

Figure 11. Relative radioelement concentrations for each intrusion displayed in ternary diagrams. Data points are sampled data from the airborne survey.

With respect to the magnetic profile, the TMA remained almost constant, situated between -50 and 0 nT. A local low is observed near the center of the carbonatite while the RTP-TMA displayed a local peak at the same position, even though it is an attenuated response in relation to the TMA data. This finding and the TMA gridded data (Fig. 3A) are contrary to previous

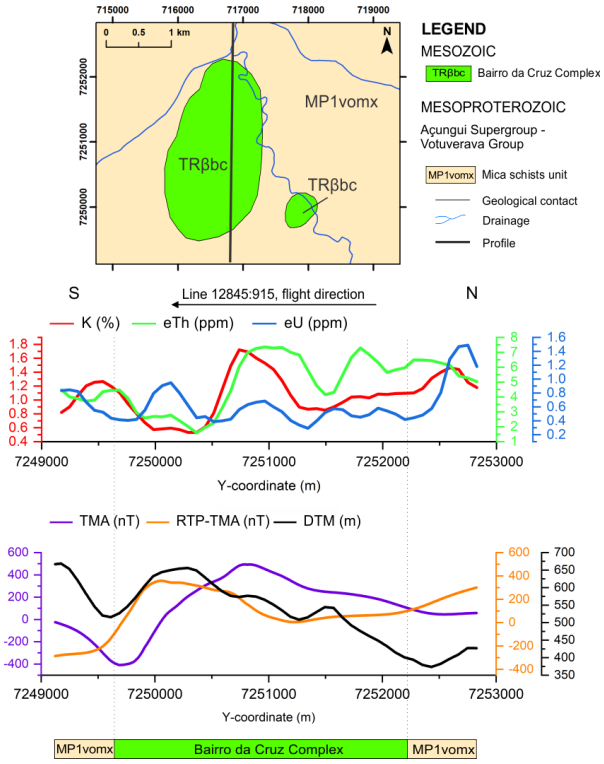

Figure 12. Flight line L12845:915 profile for radioelements (K, eTh, and eU) and magnetic data (TMA, RTP-TMA) alongside DTM values from Bairro da Cruz Complex.

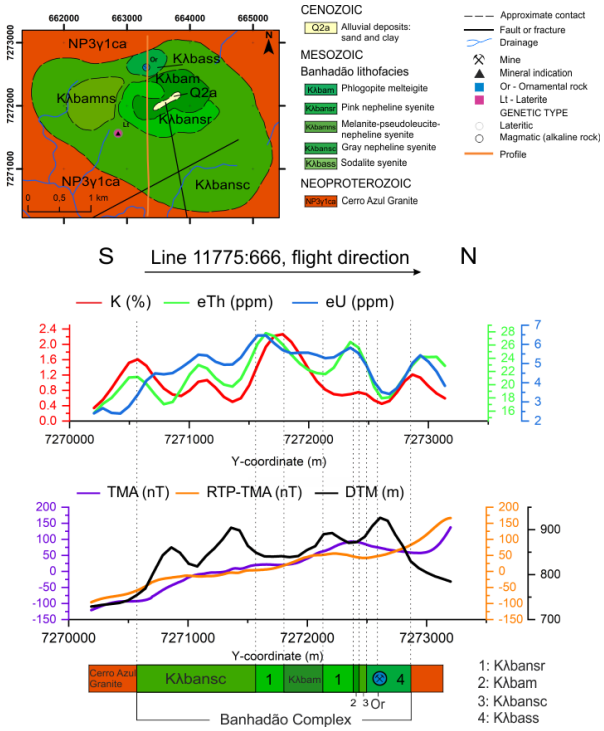

Figure 13. Flight line L11775:666 profile for radioelements (K, eTh, and eU) and magnetic data (TMA, RTP-TMA) alongside DTM values from Banhadão Complex.

studies (Drenth 2014, Thomas *et al.* 2016) which have suggested that carbonatite intrusions have circular, oval, strong magnetic signatures in their edges. However, the local low TMA in the profile (Fig. 15) is somewhat consistent with those authors' claims that carbonatite cores coincide with magnetic lows.

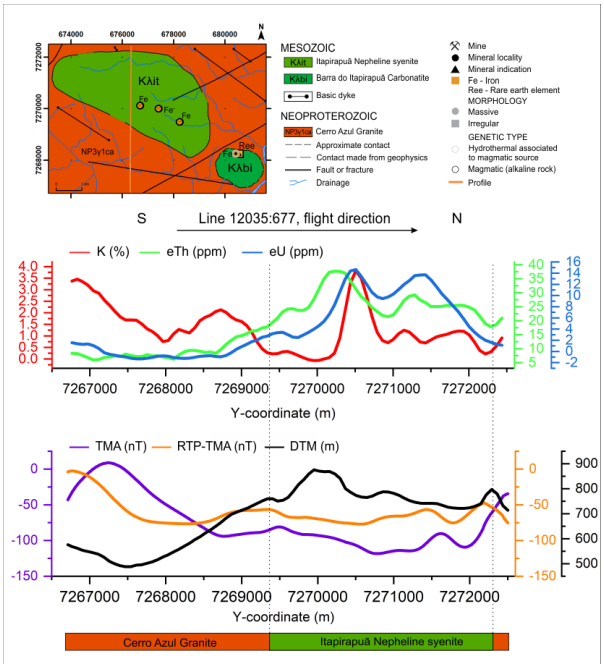

Figure 14. Flight line L12035:677 profile for radioelements (K, eTh, and eU) and magnetic data (TMA, RTP-TMA) alongside DTM values from Itapirapuã Nepheline syenite.

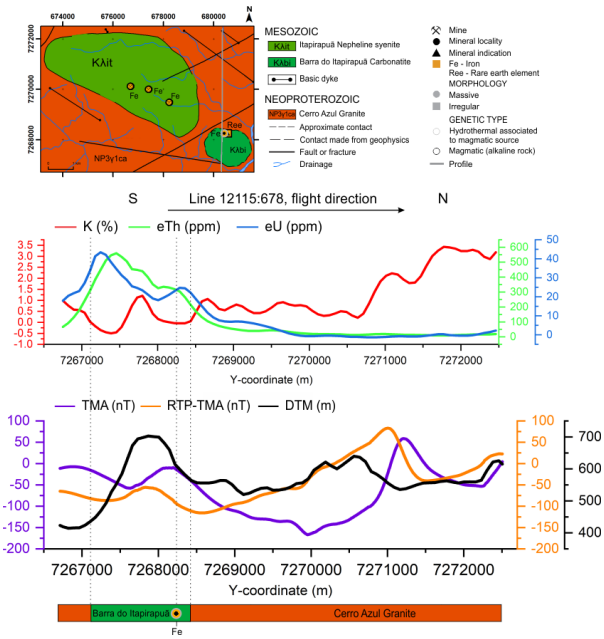

Figure 15. Flight line L12115:678 profile for radioelements (K, eTh, and eU) and magnetic data (TMA, RTP-TMA) alongside DTM values from Barra do Itapirapuã Carbonatite.

No correlation was detected between the Fe and REE mineralizations and the radiometric/magnetic responses in the BIT profile.

Barra do Teixeira Phonolite

K distributions for the BT are situated between 0.25 and 1.75 % while eTh and eU figures range from 7 to 10 ppm and 1.5 to 2 ppm, respectively (Fig. 16). The southern part of the phonolite is characterized by showing higher values of eU while there is a decrease of K and eTh from the south to the central

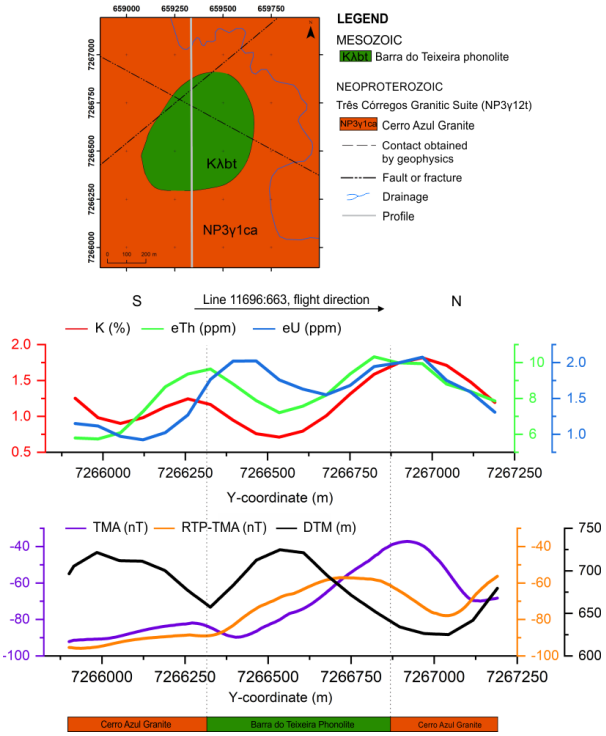

Figure 16. Flight line L11696:663 profile for radioelements (K, eTh, and eU) and magnetic data (TMA, RTP-TMA) alongside DTM values from Barra do Teixeira Phonolite.

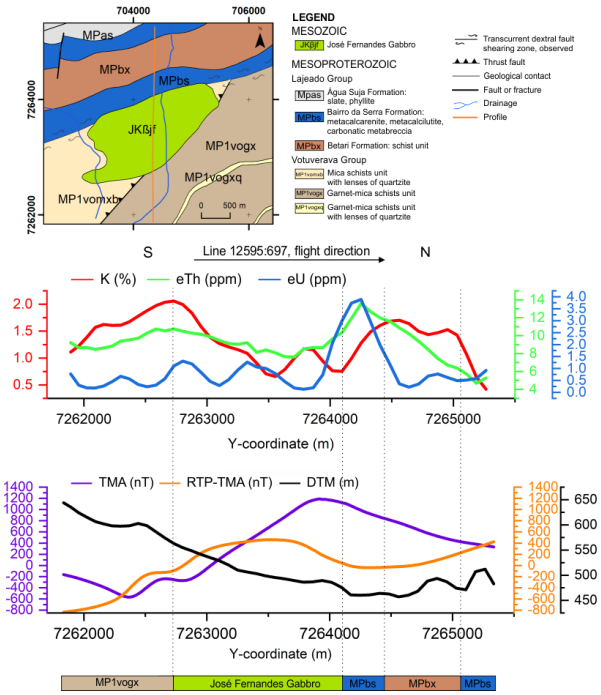

Figure 17. Flight line L12595:697 profile for radioelements (K, eTh, and eU) and magnetic data (TMA, RTP-TMA) alongside DTM values from José Fernandes Gabbro.

part of this body. There is a sharp rise of K along with eTh in the northern region of the BT profile that continued into the Cerro Azul Granite. Overall, higher radioactive element concentrations are situated near the edges of the phonolite.

The entire profile demonstrated negative values of TMA, ranging from -90 to -40 nT. The RTP-TMA data showed similar results. However, its profile seems attenuated in comparison with the TMA and has positioned the peak of this response over the center of the BT phonolite.

José Fernandes Gabbro

Along the N-S JF Gabbro profile (Fig. 17), maximum and minimum values inside this suite are 0.75–2.0 % K, 8–10 ppm eTh and 0.25–3.5 ppm eU. The lowest radioelement values of the profile are positioned over the JF suite, mostly to its central part. In this region, K and eTh levels decline from south to north while eU displays a local high, but three times lower than the peak of the Bairro da Serra Formation (MPbs), the highest for this radioelement along the profile.

The range of TMA data for the JF gabbro boundaries is -200 to 1,200 nT. This anomaly was characterized as having normal polarity for the Earth's southern hemisphere (Fig. 6A) while its RTP-TMA response has positioned a peak over the central part of the body, even though there is an attenuation of more than 600 nT in comparison with the TMA highest value.

Mato Preto Complex

Two profiles are illustrated for the MP Complex, one for its western area (Fig. 18) and another for its eastern counterpart (Fig. 19).

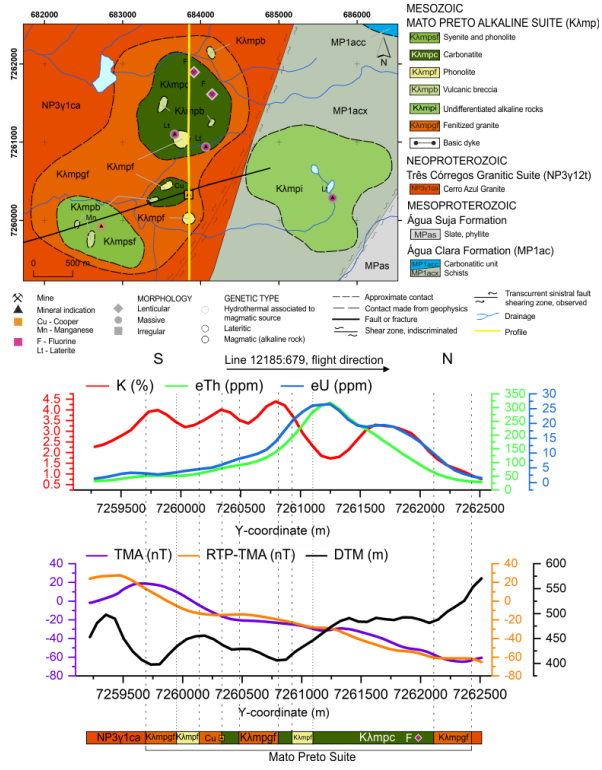

Figure 18. Flight line L12185:679 profile for radioelements (K, eTh, and eU) and magnetic data (TMA, RTP-TMA) alongside DTM values from Mato Preto Complex.

The profile located on the MP western portion (Fig. 18) comprised K, eTh, and eU concentrations varying from 2.0–4.5 %, 50–325 ppm, and 2.5–27.5 ppm, respectively. The most remarkable result is that there is a steady increase northward of eTh and eU reaching their maximum concentrations in the carbonatite lithofacies (KΛmpc) while the lowest potassium

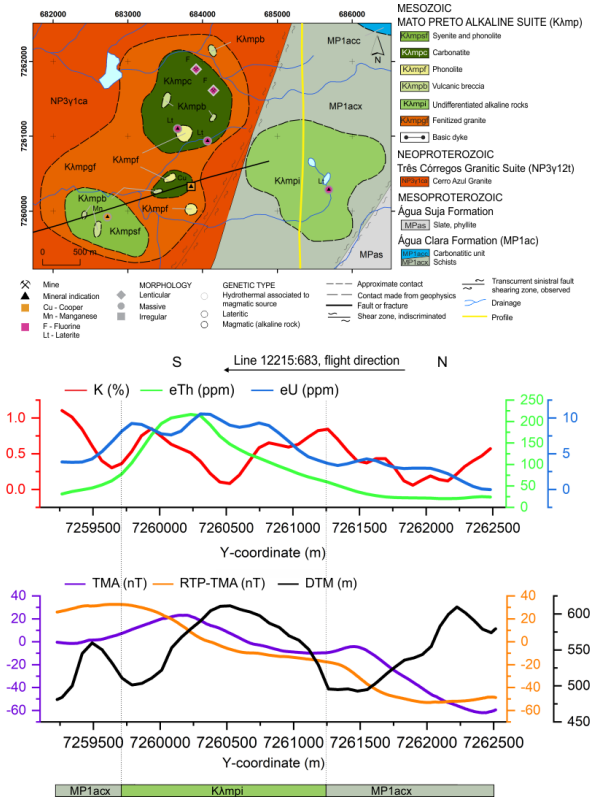

Figure 19. Flight line L12215:683 profile for radioelements (K, eTh, and eU) and magnetic data (TMA, RTP-TMA) alongside DTM values from Mato Preto Complex.

levels are located over this eTh and eU maxima. This is in good agreement with the profile of the BIT carbonatite (Fig. 15), which showed a similar pattern for these radioelement distributions, *i.e.* high contents of eTh and eU with low levels of juxtaposed potassium . The detection of different lithotypes in the MP complex may be seen only in the potassium profile, where there are some slight increases and decreases in its concentration.

Responses from TMA and RTP-TMA (Fig. 18) displayed a smooth decrease of magnetic signal from south to north in the MP suite. Starting around 20 nT, the signal slowly dropped until achieving over -60 nT in the northern portion. It is worth noting that the RTP of this signal has demonstrated virtually an identical response, both in shape and values, of TMA data. Correlations between the radiometric and magnetic data and copper and fluorine mineralizations were not observed along the profile.

The eastern portion of MP is comprised only by the undifferentiated alkaline rocks unit (KΛmpi). Its profile (Fig. 19) has the highest concentrations of eTh and eU in comparison with its country rock, schists from Água Clara Formation. Registering around 225 ppm eTh and 10 ppm eU, these peaks are situated in the central-south area of the MP suite. Like its eastern counterpart, there is a potassium depletion (around 0.25 %) stacked in the same position of eTh and eU peaks. This response seems consonant with a carbonatite radiometric signature (*i.e.* eTh and eU highs and K lows with unusual values of eTh, above 100 ppm), hence indicating that the undifferentiated alkaline rocks unit (KΛmpi) could host carbonatite bodies.

On the matter of its magnetic profile, the undifferentiated alkaline rocks unit showed a small amplitude interval from the TMA response. The minimum found was around -10 nT (in the north) while its maximum was 20 nT approximately (in the south). Moreover, this positive peak is located in the same position as the eTh highest levels.

Tunas Complex

Both profiles from Tunas (Figs. 20 and 21) could be characterized as the most erratic series among the complexes studied in this work. They displayed a large variety of ups and downs along the radiometric and magnetic data. This result may be explained by the fact that those profiles comprise different rock types, including quaternary deposits, and also by the abrupt changes observed in the digital terrain model data. This variation in the DTM could influence the geomorphic processes and thus the rock/soil responses of gamma-rays (Wilford *et al.* 1997).

Line 12325:684 profile (Fig. 20) demonstrated the highest levels of eTh and eU inside the western Tunas Complex. These concentrations, approximately 22.5 and 5 ppm, respectively, are located on the syenite and alkaline syenite unit (KΛtns). This lithotype also carries the lowest quantities of K in the profile, *i.e.* almost 0.0 to 0.5 %. This radioelement increased in the Monzodiorite and diorite unit (KΛtnd), even though its concentration is lesser than in Tunas country rocks.

The magnetic data for this profile (Fig. 20) has a significant amplitude. The TMA data has a maximum above 300 nT, which coincides with the highest levels of eTh and eU, and a minimum of -50 nT. The anomaly starts negative in the south and then steadily rises to positive values northward until changes to negative in the northernmost part of Tunas Complex. Although considerable attenuation has been observed for the RTP-TMA profile, it has peaked near the central axis of the TMA anomaly (between 7238250 and 7239000 coordinates).

Similar to its western profile, eTh and eU top levels in the eastern profile (Fig. 21) are placed in the syenite and alkaline syenite (KΛtns) lithofacies. Equivalent thorium results are 14 ppm with a local low of around 9 ppm in the center of this unit while eU erratic increase from south to north, peaking almost 3 ppm inside of KΛtns lithofacies. K quantities for Tunas eastern portion are somewhat higher, above 1.0 to 1.5 ppm, than in the western region. In addition, K concentrations in the syenite and alkaline syenite (KΛtns) lithofacies are higher than Tunas country rocks in the eastern profile, while the opposite is seen in the western profile (Fig. 20).

The eastern part of Tunas is magnetically stronger than its western region. The TMA profile showed peak to peak values around -300 nT and 1,500 nT, an amplitude interval five times higher than the one demonstrated in the western profile (Fig. 20). Additionally, the pole-reduced signal in the eastern profile did not show any substantial attenuation in contrast to the western counterpart of Tunas.

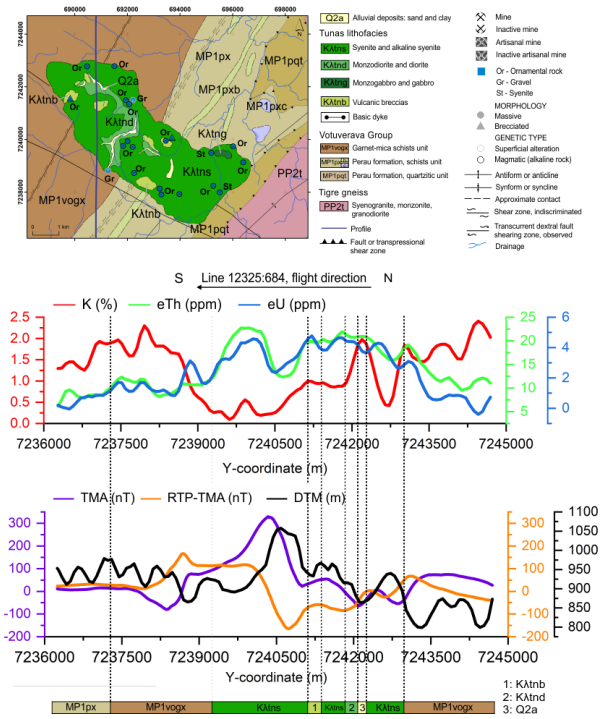

Figure 20. Flight line L12325:684 profile for radioelements (K, eTh, and eU) and magnetic data (TMA, RTP-TMA) alongside DTM values from Tunas Complex.

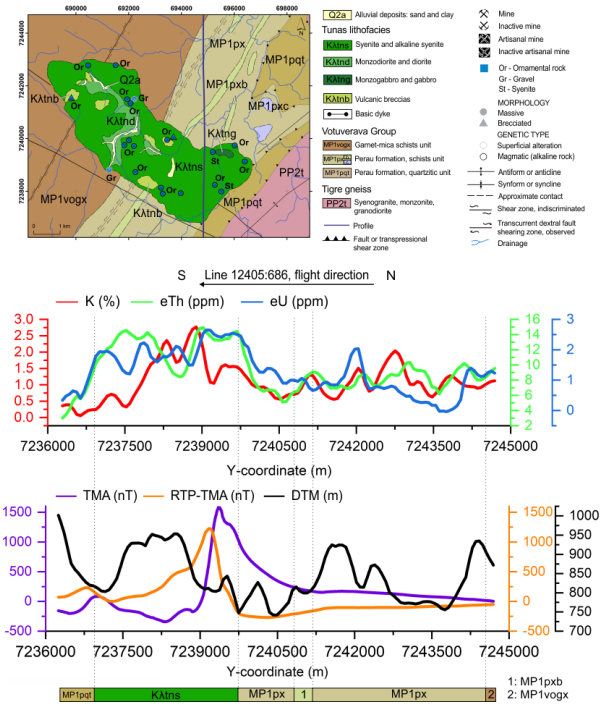

Figure 21. Flight line L12405:686 profile for radioelements (K, eTh, and eU) and magnetic data (TMA, RTP-TMA) alongside DTM values from Tunas Complex.

CONCLUSIONS

High-resolution airborne geophysical data provides a powerful component for geological interpretation when the rocks of interest did not have borehole data or access to their outcropped area is difficult. Prior works have documented geophysical evaluation of alkaline provinces in Brazil. However, these studies have not focused on magnetic and radiometric data, especially the latter. In this work, we geophysically characterized the Ponta Grossa Arch Alkaline Province, whose extent has been targeted to mineral exploration for several decades.

Modeling showed good agreement with magnetic susceptibilities values of alkaline rocks and gabbros reported in the literature, even though the shape and geometry of the PGAAP rocks could not be representative of the known geology. Further research should be carried out to establish the magnetization vector from the rocks modeled in this study as well as to confirm the intensity of remanent magnetism in those to assist in constrain inversions.

Our analyses displayed that these rocks are enriched in eTh in relation to eU and K, which supports other works regarding alkaline complexes (Ford *et al.* 1988, Verplanck and Gosen 2011, Airo 2015). In addition, we found the radiometric data useful to distinguish complexes that host carbonatites from those that do not contain them since the alkaline-carbonatitic bodies' profile data showed coincidental eTh and eU highs and K lows in which the eTh values are above 100 ppm. However, our approach to create a general classification based on radioelements for alkaline rocks was unsuccessful due to the lack of clear patterns. More information on radiometric data, such as conducting small-scale ground geophysical surveys, would help us to establish a greater degree of accuracy on this matter. Most notably, this is the first study to our knowledge to investigate in a more detailed way the magnetic and radiometric responses from alkaline bodies in the Ponta Grossa Arch, thus it has contributed to the understanding of geophysical signatures of alkaline provinces.

ACKNOWLEDGMENTS

We thank the Geological Survey of Brazil (CPRM) for providing the airborne geophysical data. F.J.F. Ferreira was supported in this research by the National Council for Scientific and Technological Development (CNPq, Brazil) (contract 303826/2018-5). We also thank Editor-in-Chief C. Riccomini and two anonymous reviewers for their comments that improved the quality of the manuscript.

ARTICLE INFORMATION

Manuscript ID: 20200051. Received on: 06/21/2020. Approved on: 04/12/2021.

V.S. wrote the manuscript and prepared all the figures and Supplementary material; F.F. provided advisorship regarding Brazilian alkaline rocks geology and geophysics, revised and improved the manuscript.

Competing interests: The authors declare no competing interests.

REFERENCES

Airo M. 2015. Geophysical signatures of mineral deposit types – synopsis. *In*: Airo M. (ed.). *Geophysical signatures of mineral deposit types*. Espoo, Geological Survey of Finland, Special Paper, 58, p. 9-70. Available at: http://tupa.gtk.fi/julkaisu/specialpaper/sp_058.pdf. Accessed on: Jul. 13, 2018.

Airo M., Hyvönen E., Lerssi J., Leväniemi H., Routsalainen A. 2014. Tips and tools for the application of GTK's airborne geophysical data. Espoo, Geological Survey of Finland, *Report of Investigation*, 215, 33 p. Available at: tupa.gtk.fi/julkaisu/tutkimusraportti/tr_215.pdf. Accessed on: Jul. 13, 2018.

Algarte J.P. 1972. A influência dos arqueamentos cratônicos no condicionamento das alcalinas dos Estados de São Paulo e Paraná. *In*: Congresso Brasileiro de Geologia, 26., Belém. *Proceedings*, v. 1, p. 65-69.

Almeida F.F.M. 1983. Relações tectônicas das rochas alcalinas mesozóicas da região meridional da plataforma sul-americana. *Revista Brasileira de Geociências*, **13**(3):139-158. https://doi.org/10.25249/0375-7536.1983133139158

Almeida V.V. 2016. *Petrologia do Gabro José Fernandes e sua relação temporal com o magmatismo mesozoico toleítico e alcalino no arco de Ponta Grossa*. PhD Thesis, Universidade de São Paulo, São Paulo, 274 p. http://doi.org/10.11606/T.44.2017.tde-30032017-083933

Almeida V.V., Janasi V.A., Azzone R.G., Faleiros F.M. 2019. Crustal contamination and genesis of transitional alkaline-tholeiitic intrusions: Insights from the José Fernandes Suite, Paraná Magmatic Province, Brazil. *Lithos*, **342-343**:59-75. https://doi.org/10.1016/j.lithos.2019.05.023

Alva-Valdivia L.M., López-Loera H. 2011. A review of iron oxide transformations, rock magnetism and interpretation of magnetic anomalies: El Morro Mine (Brazil), a case study. *Geofísica Internacional*, **50**(3):341-362. Available at: http://www.scielo.org.mx/scielo.php?script=sci_arttext&pid=S0016-71692011000300007&lng=es&nrm=iso. Accessed on: Jan. 20, 2020.

Baranov V. 1957. A new method for interpretation of aeromagnetic maps: pseudo-gravimetric anomalies. *Geophysics*, **22**(2):359-383. https://doi.org/10.1190/1.1438369

Baranov V., Naudy H. 1964. Numerical calculation of the formula of reduction to the magnetic pole. *Geophysics*, **29**(1):67-79. https://doi.org/10.1190/1.1439334

Brandt D., Hartmann G.A., Yokoyama E., Catelani E.L., Trindade R.I.F. 2009. Paleointensity data from Early Cretaceous Ponta Grossa dikes (Brazil) using a multisample method. *Earth, Planets and Space*, **61**(1):41-49. https://doi.org/10.1186/BF03352883

Briggs I.C. 1974. Machine contouring using minimum curvature. *Geophysics*, **39**(1):39-48. https://doi.org/10.1190/1.1440410

Brumatti M., Almeida V.V. 2014. *Rochas Alcalinas:* Áreas de Registro, Iguape e Cerro Azul. Anexo III: Atualização da cartografia geológica da Folha Cerro Azul SG.22-X-B-IV. Estados de São Paulo e Paraná, escala 1:100000. São Paulo: Geological Survey of Brazil. Available at: http://rigeo.cprm.gov.br/xmlui/handle/doc/17754?show=full. Accessed on: Apr. 30, 2018.

Brumatti M., Almeida V.V., Lopes A.P., Campos F.F., Perrotta M.M., Mendes D., Pinto L.G.R., Palmeira L.C.M. 2015. Metalogenia das províncias minerais do Brasil: rochas alcalinas da porção meridional do cinturão Ribeira, estados de São Paulo e Paraná. Geological Survey of Brazil, *Informe de Recursos Minerais*, Série Províncias Minerais do Brasil, v. 6, p. 1-79. Available at: http://rigeo.cprm.gov.br/xmlui/handle/doc/17432. Accessed on: Apr. 30, 2018.

Brumatti M., Tomita S.A. 2014. *Mapa geológico da folha Vila Branca – SG.22-X-B-IV-1, escala 1:50000*. São Paulo: Geological Survey of Brazil. Available at: http://rigeo.cprm.gov.br/xmlui/handle/doc/17759?show=full. Accessed on: May 7, 2018.

Clark D.A. 1997. Magnetic petrophysics and magnetic petrology: aids to geological interpretation of magnetic surveys. *AGSO Journal of Australian Geology and Geophysics*, **17**(2):83-103. Available at: http://pid.geoscience.gov.au/dataset/ga/81495. Accessed on: Jun. 26, 2019.

Clark D.A. 1999. Magnetic petrology of igneous intrusions: implications for exploration and magnetic interpretation. *Exploration Geophysics*, **30**(1-2):5-26. https://doi.org/10.1071/EG999005

Clark D.A., Emerson D.W. 1991. Notes on rock magnetization characteristics in applied geophysical studies. *Exploration Geophysics*, **22**(3):547-555. https://doi.org/10.1071/EG991547

Comin-Chiaramonti P., Gomes C.B. (eds.). 2005. *Mesozoic to Cenozoic alkaline magmatism in the Brazilian Platform*. São Paulo: EdUSP/Fapesp, 752 p.

Comin-Chiaramonti P., Gomes C.B., Ruberti E., Antonini P., Censi P. 2001. Mato Preto alkaline-carbonatite complex: geochemistry and isotope (O-C, Sr-Nd) constraints. *Geochimica Brasiliensis*, **15**:23-24. 1

Cordani U.G., Hasui Y. 1968. Idades K-Ar de rochas alcalinas do primeiro planalto do Estado do Paraná. *In*: Congresso Brasileiro de Geologia, 22., Belo Horizonte. *Proceedings*, v. 1, p. 149-153.

Drenth B.J. 2014. Geophysical expression of a buried niobium and rare earth element deposit: The Elk Creek carbonatite, Nebraska, USA. *Interpretation*, **2**(4):SJ23-SJ33. https://doi.org/10.1190/int-2014-0002.1

Dutra A.C., Marangoni Y.R., Junqueira-Brod T.C. 2012. Investigation of the Goiás Alkaline Province, Central Brazil: Application of gravity and magnetic methods. *Journal of South American Earth Sciences*, **33**(1):43-55. https://doi.org/10.1016/j.jsames.2011.06.004

Efimov A.V. 1978. Multiplikativniyi pokazatel dlja vydelenija endogennych rud aerogamma-spectrometriceskim dannym. *In*: Metody rudnoj geofiziki. Leningrado, Naucno proizvodstvennoje objedinenie geofizica, p. 59-68.

Ferreira F.J.F. 1982. *Integração de dados aeromagnéticos e geológicos: configuração e evolução tectônica do Arco de Ponta Grossa*. MS Dissertation, Universidade de São Paulo, São Paulo, 186 p. https://doi.org/10.11606/d.44.1983.tde-14082013-161535

Ferreira F.J.F., Algarte J.P. 1979. O comportamento aeromagnetométrico-cintilométrico das principais rochas alcalinas dos Estados de São Paulo e Paraná. *In*: Simpósio Regional de Geologia, 2., Rio Claro. *Proceedings*, v. 2, p. 195-208.

Ferreira F.J.F., Algarte J.P., Theodorovicz A., Martins F.A.G., Monma R., Silva R.B., Tassinari C.G.C., Rodrigues E.P., Coutinho J.V.M. 1987. O complexo alcalino de Pariquera-Açu. *In*: Simpósio Regional de Geologia, 6., Rio Claro. *Proceedings*, v. 1, p. 159-171.

Ferreira F.J.F., Fruchting A., Guimarães G.B., Alves L.S., Martin V.M.O., Ulbrich H.H.G.J. 2009. Levantamentos Gamaespectrométricos em Granitos Diferenciados. II: O Exemplo do Granito Joaquim Murtinho, Complexo Granítico Cunhaporanga, Paraná. *Geologia USP. Série Científica*, **9**(1):55-72. https://doi.org/10.5327/z1519-874x2009000100004

Ferreira F.J.F., Moraes R.A.V., Ferrari M.P., Vianna R.B. 1981. Contribuição ao estudo do Alinhamento Estrutural de Guapiara. *In*: Simpósio Regional de Geologia, 3., São Paulo. *Proceedings*, v. 1, p. 226-240.

Fitton J.G., Upton B.G.J. (eds.). 1987. *Alkaline igneous rocks*. Geological Society, 30, 568 p.

Ford K.L., Dilabio R.N.W., Rencz A.N. 1988. Geological, geophysical and geochemical studies around the Allan Lake carbonatite, Algonquin Park, Ontario. *Journal of Geochemical Exploration*, **30**(1-3):99-121. https://doi.org/10.1016/0375-6742(88)90054-4

Forman J.M.A., Angeiras A.G. 1981. Poços de Calderas and Itataia: Two case histories of uranium exploration in Brazil. *In*: International Atomic Energy Agency. Uranium Exploration Case Histories, p. 99-139.

Galbraith J.H., Saunders D.F. 1983. Rock classification by characteristics of aerial gamma-ray measurements. *Journal of Geochemical Exploration*, **18**(1):49-73. https://doi.org/10.1016/0375-6742(83)90080-8

Geological Survey of Brazil (CPRM). 1978. *Projeto Aerogeofísico Serra do Mar Sul*. Rio de Janeiro: CPRM/DNPM. Available at: http://rigeo.cprm.gov.br/xmlui/handle/doc/8583. Accessed on: Jul. 30, 2018.

Geological Survey of Brazil (CPRM). 2011. *Programa Geologia do Brasil (PGB) – Projeto aerogeofísico Paraná-Santa Catarina:* relatório final do levantamento e processamento dos dados magnetométricos e gamaespectrométricos. Lasa Prospecções. v. I. 326 p. Available at: http://rigeo.cprm.gov.br/xmlui/handle/doc/11241?show=full. Accessed on: Apr. 30, 2018.

Gnojek I., Prichystal A. 1985. A new zinc mineralization detected by airborne gamma-ray spectrometry in Northern Moravia (Czechoslovakia). *Geoexploration*, **23**(4):491-502. https://doi.org/10.1016/0016-7142(85)90076-6

Gomes C.B. 1970. Petrologia do maciço alcalino de Itapirapuã, São Paulo. *Boletim do Instituto de Geociências e Astronomia da USP*, **1**:77-188. https://doi.org/10.11606/issn.2316-9001.v1i0p77-197

Gomes C.B., Azzone R.G., Ruberti E., Vasconcelos P.M., Sato K., Rojas G.E.E. 2018. New age determinations for the Banhadão and Itapirapuã complexes in the Ribeira Valley, southern Brazil. *Brazilian Journal of Geology*, **48**(2):1-12. https://doi.org/10.1590/2317-4889201820170094

Gomes C.B., Barbieri M., Beccaluva L., Brotzu P., Conte A., Garbarino C., Macciotta G., Melluso L., Morbidelli L., Ruberti E., Scheibe L.F., Tamura R.M., Traversa G. 1987. Petrological and geochemical studies of alkaline rocks from continental Brazil: 2. The Tunas massif, State of Paraná. *Geochimica Brasiliensis*, **1**(2):201-234.

Gomes C.B., Comin-Chiaramonti P. 2005. An introduction to the alkaline and alkaline carbonatitic magmatism in and around the Paraná Basin. *In*: Gomes C.B. & Comin-Chiaramonti P. (eds.). *Mesozoic to Cenozoic Alkaline Magmatism in the Brazilian Platform*. EdUSP/Fapesp, p. 21-29.

Gomes C.B., Comin-Chiaramonti P. (eds.). 2017. *Magmatismo alcalino continental da região meridional da plataforma brasileira*. São Paulo: EdUSP/Fapesp, 608 p.

Gomes C.B., Ruberti E., Comin-Chiaramonti P., Azzone R.G. 2011. Alkaline magmatism in the Ponta Grossa Arch, SE Brazil: a review. *Journal of South American Earth Sciences*, **32**(2):152-168. http://dx.doi.org/10.1016/j.jsames.2011.05.003

Grant J.A. 1998. Ten things the textbooks don't tell you about processing and archiving airborne gamma-ray spectrometric data. *In*: Geological Survey of Canada. *Current Research n. 1998-D, Eastern Canada and national and general programs*, p. 83-87. https://doi.org/10.4095/209538

Hama M., Algarte J.P., Paiva I.P., Rodrigues J.C. 1977. Idades K/Ar do maciço alcalino do Banhadão e do complexo Bairro da Cruz. *In*: Simpósio Regional de Geologia, 1., São Paulo. *Proceedings*, v. 1, p. 170-178.

Horsfall K.R. 1997. Airborne magnetic and gamma ray data acquisition. *AGSO Journal of Australian Geology & Geophysics*, **17**(2):159-174. http://pid.geoscience.gov.au/dataset/ga/81489

Kaefer L.Q., Algarte J.P. 1972. Maciço alcalino do Banhadão: estudos preliminares. *In*: Congresso Brasileiro de Geologia, 26., Belém. *Proceedings*, v. 1, p. 55-64.

Killeen P.G. 1979. Gamma ray spectrometric methods in uranium exploration-application and interpretation. *In*: Hood P.J. (ed.). *Geophysics and geochemistry in the search for metallic ores*. Geological Survey of Canada, Economic Geology Report, 31, p. 163-230. http://dx.doi.org/10.4095/106049

Leão-Santos M., Li Y., Moraes R. 2015. Application of 3D magnetic amplitude inversion to iron oxide-copper-gold deposits at low magnetic latitudes: A case study from Carajás Mineral Province, Brazil. *Geophysics*, **80**(2):B13-B22. https://doi.org/10.1190/geo2014-0082.1

Li Y. 2017. From Susceptibility to Magnetization: Advances in the 3D Inversion of Magnetic Data in the Presence of Significant Remanent Magnetization. *In*: Tschirhart V., Thomas M.D. (eds.). Sixth Decennial International Conference on Mineral Exploration. *Proceedings of Exploration 17*, p. 239-260.

Li Y., Oldenburg D.W. 1996. 3-D Inversion of Magnetic Data. *Geophysics*, **61**(2):394-408. http://dx.doi.org/10.1190/1.1443968

Li Y., Shearer S.E., Haney M.M., Dannemiller N. 2007. Practical Methods for Interpreting Magnetic Data Affected by Strong Remanent Magnetization. *In*: Proceedings of Exploration 07: Fifth Decennial International Conference on Mineral Exploration, p. 1095-1098. Available at: http://www.dmec.ca/ex07-dvd/E07/pdfs/102.pdf. Accessed on: Oct. 19, 2018.

Li Y., Shearer S.E., Haney M.M., Dannemiller N. 2010. Comprehensive approaches to 3D inversion of magnetic data affected by remanent magnetization. *Geophysics*, **75**(1):L1-L11. https://doi.org/10.1190/1.3294766

Loureiro F.E.L., Tavares J.R. 1983. Duas novas ocorrências de carbonatitos: Mato Preto e Barra do Rio Itapirapuã. *Revista Brasileira de Geociências*, **13**(1):7-11. https://doi.org/10.25249/0375-7536.19831310711

Louro V.H.A, Mantovani M.S.M., Ribeiro V.B. 2017. Integrated geologic and geophysical interpretation of the Buraco da Velha copper deposit (Rondônia, Brazil): A basis for exploring in related environments. *Geophysics*, **82**(3):B121-B133. https://doi.org/10.1190/geo2016-0345.1

Louro V.H.A., Negrão A.P., Castro L.G., Ferreira F.J.F. 2019. Canoas geophysical anomaly: A possible alkaline body or unusual anomaly caused by mafic dykes in the Ponta Grossa Arch, Brazil? *Journal of Applied Geophysics*, **170**:103857. https://doi.org/10.1016/j.jappgeo.2019.103857

Mantovani M.S.M., Louro V.H.A., Ribeiro V.B., Requejo H.S., Santos R.P.Z. 2016. Geophysical analysis of Catalão I alkaline–carbonatite complex in Goiás, Brazil. *Geophysical Prospecting*, **64**(1):216-227. https://doi.org/10.1111/1365-2478.12283

Mantovani M.S.M., Rugenski A., Diogo L.A., Shukowsky W. 2005. Integrated geophysical investigation of a possible new alkaline occurrence in SE Brazil. *Journal of South American Earth Sciences*, **20**(3):259-266. https://doi.org/10.1016/j.jsames.2005.05.011

Marangoni Y.R., Mantovani M.S.M. 2013. Geophysical signatures of the alkaline intrusions bordering the Paraná Basin. *Journal of South American Earth Sciences*, **41**:83-89. https://doi.org/10.1016/j.jsames.2012.08.004

Morais S.M., Faleiros F.M., Costa V.S., Gomes S.D., Chieregati L.A., Rodrigues S.W.O. 2012. *Mapa geológico da Folha Apiaí, escala 1:100000*. Geological Survey of Brazil. Available at: http://rigeo.cprm.gov.br/xmlui/handle/doc/11366?show=full. Accessed on: May 3, 2018.

Paine J., Haederle M., Flis M. 2001. Using transformed TMI data to invert for remanently magnetised bodies. *Exploration Geophysics*, **32**(3-4):238-242. https://doi.org/10.1071/eg01238

Pereira W.R., Mantovani M.S.M., Santos R.P.Z. 2010. Análise geofísica do complexo Alcalino do Barreiro, Araxá-MG. *In*: Simpósio Brasileiro de Geofísica, 4. *Proceedings*, p. 1-5. https://doi.org/10.22564/4simbgf2010.038

Piccirillo E.M., Bellieni G., Cavazzini G., Comin-Chiaramonti P., Petrini R., Melfi A.J., Pinese J.P.P., Zantedeschi P., De Min A. 1990. Lower Cretaceous dyke swarms from the Ponta Grossa Arch: Petrology, Sr-Nd isotopes and genetic relationships with the Paraná flood volcanics. *Chemical Geology*, **89**(1-2):19-48. https://doi.org/10.1016/0009-2541(90)90058-F

Piccirillo E.M., Melfi A.J. (eds.). 1988. *The Mesozoic flood volcanism from the Paraná Basin (Brazil)*. Petrogenetic and geophysical aspects. São Paulo: Universidade de São Paulo, 600 p.

Pilkington M., Beiki M. 2013. Mitigating remanent magnetization effects in magnetic data using the normalized source strength. *Geophysics*, **78**(3):J25-J32. https://doi.org/10.1190/geo2012-0225.1

Raposo M.I.B., Ernesto M. 1995. An Early Cretaceous paleomagnetic pole from Ponta Grossa dikes (Brazil): implications for the South American Mesozoic apparent polar wander path. *Journal of Geophysical Research - Solid Earth*, **100**(B10):20095-20109. https://doi.org/10.1029/95JB01681

Renne P.R., Deckart K., Ernesto M., Féraud G., Piccirillo E.M. 1996. Age of the Ponta Grossa dike swarm (Brazil), and implications to Paraná flood volcanism. *Earth and Planetary Science Letters*, **144**(1-2):199-211. https://doi.org/10.1016/0012-821X(96)00155-0

Riccomini C., Velázquez V.F., Gomes C.B. 2005. Tectonic controls of the Mesozoic and Cenozoic Alkaline Magmatism in Central-Southeastern Brazilian Platform. *In*: Gomes C.B., Comin-Chiaramonti P. (eds.). *Mesozoic to Cenozoic Alkaline Magmatism in the Brazilian Platform*. São Paulo: EdUSP/Fapesp, p. 32-55.

Ruberti E., Castorina F., Censi P., Gomes C.B., Speziale S., Comin-Chiaramonti P. 1997. REE-C-O-Sr-Nd systematic in carbonatites from Barra do Itapirapuã and Mato Preto in Southern Brazil. *In*: South American Symposium on Isotope Geology, 1., Campos do Jordão. *Proceedings*, p. 271-275.

Ruberti E., Gomes C.B., Comin-Chiaramonti P. 2005. The alkaline magmatism from the Ponta Grossa Arch. *In*: Comin-Chiaramonti P. & Gomes C.B. (eds.). *Mesozoic to Cenozoic alkaline magmatism in the Brazilian Platform*. São Paulo: EdUSP/Fapesp, p. 473-522.

Rugenski A. 2006. *Investigação geofísica dos complexos alcalinos do sul e sudeste do Brasil*. PhD Thesis, Universidade de São Paulo, São Paulo, 352 p. https://doi.org/10.11606/t.14.2019.tde-26032013-093128

Saunders D.F., Branch J.F., Thompson C.K. 1994. Tests of Australian aerial radiometric data for use in petroleum reconnaissance. *Geophysics*, **59**(3):411-419. https://doi.org/10.1190/1.1443603

Saunders D.F., Burson K.R., Branch J.F., Thompson C.K. 1993. Relation of thorium-normalized surface and aerial radiometric data to subsurface petroleum accumulations. *Geophysics*, **58**(10):1417-1427. https://doi.org/10.1190/1.1443357

Saunders D.F., Terry S.A., Thompson C.K. 1987. Test of National Uranium Resource Evaluation gamma-ray spectral data in petroleum reconnaissance, *Geophysics*, **52**(11):1547-1556. https://doi.org/10.1190/1.1442271

Siga Jr. O., Gomes C.B., Sato K., Passarelli C.R. 2007. O Maciço Alcalino de Tunas, PR: Novos Dados Geocronológicos. *Geologia USP. Série Científica*, **7**(2):71-80. https://doi.org/10.5327/Z1519-874x2007000200005

Sonoki I.K., Garda G.M. 1988. Idades K/Ar de rochas alcalinas do Brasil meridional e Paraguai oriental: compilação e adaptação às novas constantes de decaimento. *Boletim IG-USP. Série Científica*, **19**:63-85. https://doi.org/10.11606/issn.2316-8986.v19i0p63-85

Swain C.J. 1976. A FORTRAN IV program for interpolating irregularly spaced data using the difference equations for minimum curvature. *Computers & Geosciences*, **1**(4):231-240. https://doi.org/10.1016/0098-3004(76)90071-6

Thomas M.D., Ford K.L., Keating P. 2016. Review paper: Exploration geophysics for intrusion-hosted rare metals. *Geophysical Prospecting*, **64**(5):1275-1304. https://doi.org/10.1111/1365-2478.12352

Ulbrich H., Gomes C.B. 1981. Alkaline rocks from continental Brazil. *Earth-Science Reviews*, **17**(1-2):135-154. https://doi.org/10.1016/0012-8252(81)90009-x

Ussami N., Kolisnyk A., Raposo M.I.B., Ferreira F.J.F., Molina E.C., Ernesto M. 1991. Detectabilidade magnética de diques do Arco de Ponta Grossa: um estudo integrado de magnetometria terrestre/aérea e magnetismo de rocha. *Revista Brasileira de Geociências*, **21**(4):317-327. https://doi.org/10.25249/0375-7536.1991317327

Vasconcellos E.M.G. 1995. *Petrologia e geoquímica de diques e "plugs" alcalinos da região do Vale do Ribeira, divisa dos Estados do Paraná e São Paulo*. PhD Thesis, Universidade de São Paulo, São Paulo, 202 p. https://doi.org/10.11606/t.44.1995.tde-28102015-105327

Vasconcellos E.M.G., Gomes C.B. 1998. Diques e "plugs" alcalinos da região do Vale do Ribeira, Divisa dos Estados do Paraná e São Paulo: características petrográficas e geoquímicas. *Geochimica Brasiliensis*, **29**:123-143. https://doi.org/10.11606/issn.2316-8986.v29i0p97-124

Verplanck P.L., Gosen B.S.V. 2011. Carbonatite and alkaline intrusion-related rare earth element deposits - A deposit model. *U.S. Geological Survey Open-File Report 2011-1256*, 6 p. http://dx.doi.org/10.3133/ofr20111256

Vieira A.J. 1973. Geologia do centro e nordeste do Paraná e centro-sul de São Paulo. *In*: Congresso Brasileiro de Geologia, 27., Aracaju. *Proceedings*, v. 3, p. 259-277.

Wilford J.R., Bierwirth P.N., Craig M.A. 1997. Application of airborne gamma-ray spectrometry in soil/regolith mapping and applied geomorphology. *AGSO Journal of Australian Geology and Geophysics*, **17**(2):201-216. Available at: http://pid.geoscience.gov.au/dataset/ga/81503. Accessed on: Jun. 20, 2019.